HHS Public Access

Author manuscript

Sci Transl Med. Author manuscript; available in PMC 2022 September 22.

Published in final edited form as:

Sci Transl Med. 2022 June 08; 14(648): eabh1261. doi:10.1126/scitranslmed.abh1261.

Delivery of an ectonucleotidase inhibitor with ROS-responsive nanoparticles overcomes adenosine-mediated cancer immunosuppression

Chengqiong Mao[1], **Stacy Yeh**[2,†], **Juan Fu**[1,‡], **Mercedes Porosnicu**[3,4], **Alexandra Thomas**[3,4], **Gregory L. Kucera**[1,4], **Konstantinos I. Votanopoulos**[4,5], **Shaomin Tian**[6], **Xin Ming**[1,2,4,*]

[1]Department of Cancer Biology, Wake Forest University School of Medicine, Winston-Salem, NC 27157, USA.

[2]Department of Biomedical Engineering, Wake Forest University School of Medicine, Winston-Salem, NC 27157, USA.

[3]Depatment of Internal Medicine - Section of Hematology and Oncology, Wake Forest University School of Medicine, Winston-Salem, NC 27157, USA.

[4]Comprehensive Cancer Center, Wake Forest Baptist Medical Center, Winston-Salem, NC 27157, USA.

[5]Department of Surgery - Section of Surgical Oncology, Wake Forest University School of Medicine, Winston-Salem, NC 27157, USA.

[6]Department of Microbiology & Immunology, University of North Carolina at Chapel Hill, Chapel Hill, NC 27599, USA.

Abstract

Tumor evasion of immune destruction is associated with the production of immunosuppressive adenosine in the tumor microenvironment (TME). Anticancer therapies can trigger adenosine triphosphate (ATP) release from tumor cells, causing rapid formation of adenosine by the ectonucleotidases CD39 and CD73, thereafter exacerbating immunosuppression in the TME. The goal of this study was to develop an approach to facilitate cancer therapy–induced immunogenic cell death including ATP release and to limit ATP degradation into adenosine, in order to achieve

[*]Corresponding author. xming@wakehealth.edu.
[†]Present address: Department of Neurosurgery, University of Pittsburgh, Pittsburgh, PA 15260, USA.
[‡]Present address: School of Medicine, South China University of Technology, Guangzhou 510006, P. R. China.

Author contributions: C.M., S.T., and X.M. conceptualized the research studies. C.M., S.Y., S.T., J.F., and X.M. designed and developed the methodology. C.M. and X.M. designed the nanoparticle constructs. C.M., S.Y., and J.F. performed all in vitro and in vivo studies. S.Y. and X.M. performed HPLC studies. K.I.V. and G.L.K. contributed to the PDOTS design and human tumor surgical specimen collection. C.M., S.Y., J.F., S.T., and X.M. interpreted and discussed the data. C.M., S.Y., S.T., and X.M. wrote the paper. C.M., S.Y., J.F., M.P., A.T., G.L.K., K.I.V., S.T., and X.M. participated in manuscript revisions.

Competing interests: A.T. is a scientific advisory board member of Eli Lilly, Genentech. The other authors declare that they have no competing interests.

Data and materials availability: All data associated with this study are present in the paper or the Supplementary Materials. MOC cells were provided to Wake Forest University Health Sciences under a material transfer agreement with Dana-Farber Cancer Institute. H-2K^{b} SIINFEKL Tetramer was provided to Wake Forest University Health Sciences under a material transfer agreement with NIH Tetramer Core Facility, Emory University.

durable antitumor immune response. Our approach was to construct reactive oxygen species (ROS)–producing nanoparticles that carry an ectonucleotidase inhibitor ARL67156 by electronic interaction and phenylboronic ester. Upon near-infrared irradiation, nanoparticle-produced ROS induced ATP release from MOC1 cancer cells in vitro and triggered the cleavage of phenylboronic ester, facilitating the release of ARL67156 from the nanoparticles. ARL67156 prevented conversion of ATP to adenosine and enhanced anticancer immunity in an MOC1-based coculture model. We tested this approach in mouse tumor models. Nanoparticle-based ROS-responsive drug delivery reprogramed the immunogenic landscape in tumors, eliciting tumor-specific T cell responses and tumor regression, conferring long-term survival in mouse models. We demonstrated that TME reprograming sets the stage for response to anti-programmed cell death protein 1 (PD1) immunotherapy, and the combination resulted in tumor regression in a 4T1 breast cancer mouse model that was resistant to PD1 blockade. Furthermore, our approach also induced immunological effects in patient-derived organotypic tumor spheroid model, suggesting potential translation of our nanoparticle approach for treating human cancers.

INTRODUCTION

The use of immune checkpoint inhibitors (ICIs) has shifted the focus of cancer research from the tumor to the host, and the development of various forms of immunotherapy has mobilized the immune system for an effective antitumor immune response (1, 2). However, many patients with nonimmunogenic tumor microenvironments (TMEs) show resistance to ICIs (3-6). For most common solid tumors, including breast cancer, lung cancer, and head and neck cancer, only about 20% of patients respond to ICIs (1, 7, 8). This indicates that additional immunosuppressive mechanisms could be targeted to maximize therapeutic benefit (4, 9, 10). However, suppressive mechanisms usually play an essential regulatory role in the normal tissues to enforce self-tolerance and to protect against excessive immune activation and autoimmunity (11, 12). Thus, strategies that can promote an immunogenic TME and avoid severe side effects remain crucial in the development of effective and safe cancer immunotherapy (6, 13).

Purinergic signaling is an important component of immune regulation, of which adenosine triphosphate (ATP) and adenosine (Ado) are the most potent modulators of immune responses (14). The extracellular concentrations of Ado and ATP are normally low in healthy tissue (15, 16). External stimulation and stress can trigger ATP release at high concentrations from malignant cells through a variety of anticancer therapies, including chemotherapy, radiotherapy, phototherapy, and surgery (17-21). Acting as a danger signal, extracellular ATP (eATP) is involved in the recruitment and activation of both innate and adaptive immune cells by stimulation of purinergic P2 receptors (18, 22-25). As a pivotal step in the initiation of anticancer immunity, ATP release into extracellular space is considered one of the three hallmarks of immunogenic cell death (26, 27). However, eATP in the TME is quickly degraded into immunosuppressive Ado by the synchronized enzymatic activity of ectonucleotidases. These include nucleoside triphosphate diphosphohydrolases (NTPDases) such as CD39, which hydrolyze ATP to adenosine 5′-monophosphate (5′-AMP), and ecto-5′-nucleotidases, mainly CD73, which further hydrolyze 5′-AMP to Ado (22, 23, 28). Both enzymes are widely expressed in the TME and set up a negative-

feedback mechanism to prevent antitumor immunity (26, 28, 29). Tumoral Ado interacts with the purigenic P1 receptors and dampens antitumor immunity by suppressing the cytotoxicity of T cells and sustaining the activities of suppressive immune cells (30-32). Thus, despite the ability to damage tumor cells, conventional cancer therapy can produce an immunosuppressive TME enriched with Ado, leading to tumor resistance or recurrence (33-35). In the TME, a shift in balance toward ATP is crucial for initiating and maintaining an effective antitumor response. In this study, we aim to develop a combination therapy approach that, on the one hand, facilitates cancer therapy–induced immunogenic cell death including ATP release in the TME, whereas, on the other hand, limits ATP degradation into Ado, thereby achieving durable antitumor immune response.

Ectonucleotidase inhibitors that are used to inhibit ATP degradation to Ado are largely nucleotide derivatives, including ARL67156 (ARL), Adenosine 5′-(α,β-methylene)diphosphate, and PSB12379 (36). These compounds generally have a short half-life in the blood circulation (37), which prevents their accumulation to effective concentrations in the tumors. Delivery systems such as liposomes could enhance tumor delivery of nucleotide derivatives that are small molecules and highly hydrophilic (38, 39). However, specific release of those nucleotide compounds from the delivery systems in tumors remains a challenge. In addition, chemical linking of nucleotides to a delivery system for enhanced tumor delivery may not be feasible, because the active site of the nucleotide that binds to the ectonucleotidase can be readily incapacitated (36, 40).

Stimuli-responsive drug delivery is an important strategy for achieving disease-specific therapeutics and for reducing off-target toxicity (41). These delivery systems are designed to respond to specific stimuli, including heat, light, reactive oxygen species (ROS), and enzymes, for triggered release of therapeutics selectively within the diseased sites. Boronic acids (BAs) are highly promising for stimuli-responsive drug delivery because of favorable physicochemical properties under physiological conditions and low toxicity in vivo (42-45). In addition, BAs form reversible covalent esters with 1,2- or 1,3-cis-diols that are present at nucleosides and nucleotides on the ribose ring (42). We thus propose a ROS-responsive approach for specific release of nucleotide drugs, being an ectonucleotidase inhibitor ARL in this study. ARL is a potent CD39 inhibitor, which also has additional capability to block CD73, thus acting as a dual CD39/CD73 ectonucleotidase inhibitor (46). We demonstrate this approach by using a ROS-labile nanoparticle (NP), composed of BA-containing cationic polymer poly[(2-acryloyl)ethyl(p-boronic acid benzyl)diethylammonium bromide] (PDEAEA-PBA) and photosensitizer-containing lipid polymer 1,2-distearoyl-sn-glycero-3-phosphoethanolamine-*N*-[amino(polyethylene glycol)-2000]-IRDye 700 (DSPE-PEG_{2000}-IR700). In this delivery system, the photosensitizer-containing lipid polymer DSPE-PEG_{2000}-IR700 is a ROS-producing component, which is able to kill tumor cells under light irradiation and promote immunogenic cell death including ATP release in the TME. Concurrently, it provides the ROS trigger to the delivery system. The BA-containing cationic polymer is a ROS-responsive conjunction component, which links the anionic nucleotides by electronic interaction and phenylboronic ester. When the ROS-producing component generates ROS upon near-infrared (NIR) irradiation, the phenylboronic ester is cleaved and the cationic polymer is converted into an anionic polymer, facilitating ARL release in tumor sites.

In this study, we hypothesize that stimuli-responsive delivery of CD39/CD73 inhibitors can selectively reprogram the TME and provide an effective cancer immunotherapy. We constructed ROS-producing NPs carrying CD39/CD73 inhibitor ARL and photosensitizer IR700. We then tested ROS-triggered release of ARL from NPs, evaluated the capability of the NPs to induce immunogenic cell death in MOC1 cancer cells, and examined the immunological effects in a coculture model of MOC1 cells and mouse immune cells. Tumor delivery of the NPs was examined in a mouse MOC1 syngeneic oral cancer model, whereas antitumor responses and reprograming of the TME were evaluated in MOC1, MOC2 oral cancer, MC38-OVA colon cancer, and 4T1 breast cancer mouse models. The combination of PD1 blockade with our NP delivery approach was examined in anti-PD1–resistant MOC2 and 4T1 tumor models (47, 48). Last, tumor samples of patients with breast cancer or colon cancer were used to examine the potential immunological effects induced by our NP approach, suggesting future research for potential translation of our NP approach for treating human cancers.

RESULTS

Preparation and characterization of NPs

The structure of the polymers and the drug loading process are shown in Fig. 1A. We used a ROS-labile charge-reversal polymer, poly[(2-acryloyl)ethyl(p-boronic acid benzyl)diethylammonium bromide] (PDEAEA-PBA). The PDEAEA-PBA and DSPE-PEG-IR700 coassembled to form NPs (NP700), which was followed by ultrafiltration of 100-kDa molecular weight cutoff thrice (fig. S1). The NP700 showed an average hydrodynamic size of 145.6 ± 2.7 nm and zeta potential of 32.1 ± 4.5 mV as determined by dynamic light scattering (fig. S2). After loading with the ectonucleotidase inhibitor ARL, a nucleotide derivative and ATP analog with negative charge, the resultant NPs (NP700-ARL) demonstrated a decreased average hydrodynamic size of 102.8 ± 2.6 nm and reduced zeta potential of 4.1 ± 0.7 mV (Fig. 1, B and C, and fig. S2). Both NP700 and NP700-ARL showed strong IR700 fluorescence after ultrafiltration thrice, whereas DSPE-PEG-IR700 could not form stable NPs by itself and were removed gradually by ultrafiltration (fig. S1), which indicated that PDEAEA-PBA helped coassemble with DSPE-PEG-IR700. We further performed a gel retardation assay to examine the stability of the resultant NPs. A fluorescent-labeled nucleotide Alexa Fluor 546-14-UTP (UTP^{AF546}) was used in this experiment as the fluorescent characteristic of this nucleotide facilitated real-time tracking of gel migration of the nucleotide that was loaded on the NPs. As visualized with IR700 fluorescence, DSPE-PEG-IR700 migrated quickly to the front of the gel (Fig. 1D), indicating that it did not form stable NPs. The DSPE-PEG-IR700 and UTP^{AF546} in the DSPE-PEG-IR700 + UTP^{AF546} group migrated to the front of the gel and were not exactly colocalized, which further validated that DSPE-PEG-IR700 did not form stable NPs with the nucleotide UTP^{AF546}. When coassembled with PDEAEA-PBA, NP700-ARL did not migrate from the loading well in the agarose gel because of their large size (Fig. 1D). Free UTP^{AF546} migrated to the front of the gel, but NP700-UTP^{AF546} stayed in the loading well and showed colocalization with the IR700 signal (Fig. 1D), indicating that the nucleotides were tightly loaded in the NPs.

ROS induces ARL release from NP700-ARL

The premise of the NP design relies on ROS-triggered ARL release in the TME. We hypothesized that the oxidation of the carbon-boron bond by ROS by light irradiation could induce deboronation and cause PDEAEA-PBA to release p-quinone methide (HMP) and form tertiary amine, which would further self-catalyze the ester group hydrolysis and, lastly, produce anionic poly(acrylic acid) (Fig. 1A). We then thought that the charge reversal of the NPs and the deboronation would induce a triggered release of ARL. To validate this hypothesis, we first evaluated the generation of ROS and found that the IR700-containing NPs produced ROS after light irradiation (fig. S3). We further examined ROS-triggered release of ARL from the NPs. After irradiation of NP700-ARL, the samples were analyzed with high-performance liquid chromatography (HPLC) to monitor the generation of ARL in free form and HMP, which is the by-product from the PDEAEA-PBA oxidation after light irradiation (Fig. 1A). As shown in fig. S4, the zeta potential of NP700 after oxidation decreased gradually as the ester group underwent self-catalyzed hydrolysis and produced anionic poly(acrylic acid), thus achieving charge reversal from +32.1 to −17.1 mV. Furthermore, from the HPLC results in Fig. 1E and fig. S5, we observed that NIR initiated ARL release from NP700-ARL, and the released drug reached saturation at a light dose of 10 J/cm^2 [the plus sign (+) indicates light irradiation throughout the text and all the figures]. The release profile of by-product HMP was similar to that of ARL (fig. S5), indicating that the drug release was accompanied by ROS-triggered degradation of the polymer. Non-irradiated control samples did not show any evidence of drug release. These results suggest that the drug release of NP700-ARL under NIR irradiation occurs simultaneously with the ROS generation.

NP700-ARL(+) causes immunogenic cell death and promotes dendritic cell (DC) maturation

Photodynamic therapy (PDT), a Food and Drug Administration–approved cancer therapy (49), can cause ATP release and thereafter immunogenic cell death of cancer cells, resulting in favorable anticancer immunity (17). However, eATP in the TME is quickly degraded into immunosuppressive Ado by the concerted enzymatic activity of ectonucleotidases, dampening anticancer immunity (34). We hypothesized that stimuli-responsive delivery with NP700-ARL can generate ROS to activate the ARL release at tumor sites, which prevents conversion of ATP to Ado and prolongs the immunogenic actions, leading to durable antitumor response.

To test our hypothesis, we first measured extracellular release of ATP from the mouse MOC1 cell line after NIR irradiation by Luminescent assay. The four treatment groups included (i) the phosphate-buffered saline (PBS) group, (ii) the NP700-ARL group, (iii) the NP700(+) group (NP700 treatment followed by light irradiation), and (iv) the NP700-ARL(+) group (NP700-ARL treatment followed by light irradiation). As shown in fig. S6, single treatment with NP700-ARL did not cause death of MOC1 cells; however, after light irradiation, NP700-ARL(+) induced dose-dependent light toxicity. In addition, treatment with NP700-ARL(+) caused a significant increase in bioluminescent signal in ATP bioluminescence assay ($P < 0.001$; Fig. 2, A and B), indicating that photosensitizer IR700 produced light toxicity to MOC1 cells upon NIR irradiation and caused release of intracellular ATP (Fig. 2C). The treatment with NPs not carrying ARL followed by light

irradiation [NP700(+) group] produced a transient increase in eATP; however, it decayed within 4 hours, whereas the NP700-ARL(+) group preserved high eATP amounts up to 24 hours after light irradiation. This result indicated that the NP700(+) caused rapid release of ATP, but it was quickly degraded by cellular ectonucleotidases.

In addition to ATP release, calreticulin (CRT) translocation from the endoplasmic reticulum to the cell surface and extracellular high mobility group box protein 1 (HMGB1) release from the nuclei are the other hallmarks of immunogenic cell death. These actions play a role in stimulating the engulfment of dying tumor cells by immature DCs, leading to DC maturation (17). As shown in Fig. 2D, MOC1 tumor cells treated with PBS or NP700-ARL showed few cell surface CRT exposure (green); however, increased cell surface CRT exposure was observed in the NP700(+) and NP700-ARL(+) groups, which were induced by IR700-medicated PDT. The flow cytometry results shown in Fig. 2E further confirmed these results. HMGB1 release was analyzed by enzyme-linked immunosorbent assay (ELISA; Fig. 2F). Compared with the groups of PBS and NP700-ARL, the NP700(+) and NP700-ARL(+) groups showed about a fourfold increase in HMGB1 release. To test whether immunogenic cell death occurred in vivo in Babl/c or C57bl/6 mice bearing tumors after NP700-mediated phototherapy, we examined CRT expression in tumors after intravenous administration of the NPs followed by NIR irradiation. As shown in fig. S7, tumoral CRT expression was enhanced after the NP700(+) or NP700-ARL(+) treatments in MC38, MOC1, and 4T1 tumor tissues, indicating that immunogenic cell death was induced in vivo after our NP700-based phototherapy. We further treated human breast cancer and colon cancer tumor in resected surgical specimens ex vivo to examine whether NP700-ARL(+) could induce immunogenic cell death in human cells. As shown in fig. S8, the NP700-ARL(+) treatment successfully induced immunogenic cell death in both breast tumor and colon tumor cells, as indicated by increased production of eATP, HMGB1, and CRT.

We then examined the effects of NP700-ARL(+)–induced immunogenic cell death on DC maturation using in vitro assays. MOC1 cells underwent the different treatments previously mentioned. Immature DCs were added to the culture and coincubated with MOC1 cells, and then the DCs were analyzed by flow cytometry to examine the expression of major histocompatibility complex class II (MHC-II) and CD86 as markers for DC maturation. As shown in Fig. 2 (G and H), MOC1 cells treated with NP700(+) modestly increased surface expression of CD86 in the DCs ($P < 0.001$), but those undergoing the NP700-ARL(+) treatment substantially increased surface expression of both MHC-II and CD86 in the cocultured DCs ($P < 0.001$). We further examined the expression of CD39 and CD73 in DCs and found that NP700(+) and NP700-ARL(+) treatments increased CD39 expression, whereas only NP700(+) treatment up-regulated CD73 expression in the DCs (fig. S9). In addition, the NP700-ARL(+) treatment increased the production of proinflammatory cytokines IL12p40 and IL1b, but not immunosuppressive cytokine interleukin-10 (IL-10) (fig. S10). These data suggest that NP700-ARL(+) stimulates DC maturation through immunogenic cell death of cancer cells and ARL-mediated inhibition of ATP degradation.

NP700-ARL(+) promotes T cell proliferation and antigen-specific activation

ATP in the TME is quickly degraded into immunosuppressive Ado by the concerted enzymatic activity of ectonucleotidases, such as CD39 and CD73, dampening anticancer immunity (28). To examine whether CD39 and CD73 are expressed in the TME, we first collected the MOC1 tumors 14 days after tumor inoculation from the tumor-bearing mice and measured the expression of CD39 and CD73 within different immune cell subsets and cancer cells in the MOC1 tumors. As shown in Fig. 3 (A and B), we found CD39 and CD73 were widely expressed in the TME. DCs, regulatory T cells (T_{regs}), MOC1 cancer cells, and endothelial cells in the tumors expressed both CD39 and CD73, whereas $CD8^+$ T cells had relatively low expression of CD39 and CD73. Next, we isolated different cell populations from MOC1 tumors and tested the ability of each cell subset to hydrolyze eATP. As shown in Fig. 3C, all the cell subsets were able to hydrolyze eATP, although $CD8^+$ T cells showed the lowest hydrolysis activities, which was consistent with the expression profiles of CD39 and CD73 in these cells. We further measured the expression of CD39 and CD73 in mouse MC38 tumors and human breast or colon tumor surgical specimens. Similar expression profiles of CD39 and CD73 were observed in both mouse and human tumors, indicating that both ectonucleotidases were expressed in mouse and human TME (figs. S11 to S13). Moreover, we examined ectonucleotidase activities of tumor cells dissociated from mouse MOC1, 4T1, and MC38 tumor tissues, as well as human tumor tissues of patients with breast cancer or colon cancer. All tumor types showed the activities of ATP hydrolysis and Ado production (Fig. 3, D and E), consistent with the ectonucleotidase expression profiles. These results supported our hypothesis that eATP is quickly degraded into Ado by CD39 and CD73 in the TME.

To examine whether this ROS-responsive ARL delivery approach could overcome ATP hydrolysis and Ado production in the TME, we carried out a coculture experiment as shown in Fig. 3F. MOC1 cells were treated with different NPs. One hour after NIR light irradiation, the mixed $CD4^+$ and $CD8^+$ T cells that were prelabeled by carboxyfluorescein succinimidyl ester (CFSE) were added to the culture and coincubated with MOC1 cells. The supernatant was collected to determine the extracellular concentrations of ATP and Ado. As shown in Fig. 3F, the NP700(+) group showed significantly lower eATP concentration [13.3% of the NP700-ARL(+) group; $P < 0.001$] but higher Ado concentration [9.6-fold higher than the NP700-ARL(+) group; $P < 0.001$], indicating that the eATP released from tumor cells was quickly hydrolyzed to Ado after light irradiation. When tumor cells were treated with NP700-ARL(+), there was a marked reduction in ATP hydrolysis rate. We concluded that eATP hydrolysis by ectonucleotidases was largely inhibited by the triggered release ARL nanosystem.

Because the eATP amount increased whereas the Ado amount decreased in the NP700-ARL(+) treatment group, we further examined the effect of NP700-ARL(+) treatment on T cell proliferation by quantifying the CFSE dye dilution. As shown in Fig. 3G, we observed that MOC1 cells that underwent NP700(+) treatment suppressed $CD4^+$ and $CD8^+$ T cell proliferation, likely due to Ado production after ATP release and degradation. In contrast, MOC1 cells that underwent NP700-ARL(+) treatment did not suppress T cell proliferation, indicating that ROS-responsive ARL delivery offsets the negative impact of PDT by

inhibiting ectonucleotidases activity. We used an adenosine receptor (AdoR) inhibitor, ZM241385, as control to further determine the role of Ado in T cell proliferation. As shown in Fig. 3F, NP700-mediated PDT plus the AdoR inhibitor [NP700 + iAdoR(+) group] did not decrease the Ado concentration; however, it still could offset T cell proliferation arrest caused by Ado production (Fig. 3G). We further detected interferon-γ (IFN-γ) production by T cells (Fig. 3H) and found that there was no significant difference between the NP700-ARL(+)–treated group and the NP700 + iAdoR(+)–treated group ($P > 0.05$); both of them induced higher IFN-γ production compared with the PDT-only group. These results further confirmed that the T cell proliferation inhibition was caused by PDT-induced Ado production.

To examine whether NP700-ARL(+) could enhance DCs sensing and cross-presentation of tumor antigen to prime T cells, we treated MOC1-OVA cells (MOC1 cells stably expressing chicken ovalbumin) with NP700-ARL(+). The treated MOC1-OVA cells were then incubated with immature DCs (Fig. 3I). Flow cytometry analysis showed that NP700(+) led to a moderate increase in the OVA peptide–MHC-I complex on DCs (1.8-fold higher than the PBS group; $P < 0.05$), and even higher expression when DCs were coincubated with NP700-ARL(+)–treated MOC1-OVA cells (5.0-fold higher than the PBS group; $P < 0.001$; Fig. 3I). We further isolated OT-I cells from transgenic C57BL/6-Tg(TcraTcrb)1100Mjb/J mice, whose T cell receptors are engineered to specifically recognize the OVA peptide residues 257 to 264 SIINFEKL, and incubated the OT-I cells with the above mixture of DCs and MOC1-OVA cells (Fig. 3J). ELISA results showed significantly higher concentrations of IFN-γ in the culture medium where the DCs were preincubated with NP700-ARL(+)–treated MOC1-OVA cells ($P < 0.001$; Fig. 3J), indicating activation of tumor antigen–specific $CD8^+$ T cells. This demonstrates that NP700-ARL(+) efficiently promotes APC activation and cross-presentation of tumor antigen to prime effector $CD8^+$ T cells.

NPs deliver nucleotides to tumors in vivo

Fluorescent-labeled nucleotide UTP^{AF546} was used to mimic ARL and study distribution of NPs in vivo by in vivo imaging system (IVIS). NP700, NP700-UTP^{AF546}, or NP700 plus free UTP^{AF546} were intravenously injected into the luciferase-expressing MOC1 (MOC1-Luc) tumor-bearing mice. The time-dependent AF546 fluorescence (indicating nucleotide distribution) and IR700 fluorescence (indicating NP distribution) images of the mice showed unique tumor accumulation of the nucleotides that were delivered by the NPs (Fig. 4A). All the NP700-, NP700-UTP^{AF546}–, and NP700 plus free UTP^{AF546}–injected mice emitted strong IR700 signals from the tumor area starting as early as 1 hour after injection, which indicated that NP700 could successfully accumulate at the tumor tissues. However, only the NP700-UTP^{AF546}–treated group showed AF546 signals in the tumor area. NP700 plus free UTP^{AF546}–injected mice showed very poor signal of AF546 at the tumor site but emitted strong AF546 signal from the bladder. These results indicated that nucleotides in free form were quickly cleared by kidney and were unable to accumulate within the tumor tissue.

In this case, the NP-based delivery system can greatly enhance the tumor-delivering efficiency of nucleotides, as the photon intensity in tumor site increased from 32 in the NP700 plus free UTP^{AF546} group to 1262 in the NP700-UTP^{AF546} group 4 hours after

injection (Fig. 4, A and B). The IR700 and AF546 fluorescence intensity gradually increased through 8 hours after injection and then decreased slightly at 24 hours after injection in the NP700-UTP^{AF546}–treated mice (Fig. 4B). Considering that there were no significant differences in IR700 intensity in the tumor sites between 4 and 8 hours after injection ($P > 0.05$), we chose 4 hours after injection for the NIR light irradiation. The bioluminescence imaging of luciferase expression largely decreased and was almost undetectable after light treatment for all the groups receiving IR700-containing NPs (fig. S14), indicating that the photosensitizer IR700 was successfully delivered to the tumor site and activated by light to specifically kill the tumor cells. The ex vivo IVIS analysis at 8 or 24 hours after injection provided additional information about the tumor accumulation of the IR700-containing NPs and AF546-labeled nucleotides (Fig. 4, C and D). The liver is the most common off-target site of NPs, and the IR700 signals from the excised liver and tumor were consistent with in vivo IVIS images, although AF546 signals from the excised liver were stronger than in vivo images because of its low light penetration. The NP700-UTP^{AF546} group showed good tumor accumulation for both IR700 and AF546 signals up to 24 hours after injection, whereas the NP700 plus free UTP^{AF546} group only show good tumor accumulation of IR700 and scarcely delivered the nucleotides to the tumors. The majority of UTP^{AF546} in this group distributed to the kidneys, further indicating the advantages of an NP-based system for tumor delivery of nucleotides.

NP700-ARL(+) suppresses MC38 tumor growth and elicits tumor-specific immunity

Next, we explored whether treatment with NPs could modulate the tumor immune microenvironment in a subcutaneous colon cancer model. MC38-OVA tumor–bearing mice were treated with NP700-ARL(+) on days 14 and 17 after tumor inoculation, tumor growth was monitored by bioluminescence imaging (Fig. 5A), and actual tumor size was measured by caliper twice per week. As shown in Fig. 5B, the NP700-ARL treatment did not inhibit tumor growth, and the treatments of NP700(+) or NP700(+) plus free ARL [NP700 + Free ARL(+) group] partially suppressed tumor growth. The NP700-ARL(+) treatment resulted in a further decrease in tumor burden and significantly prolonged survival in MC38-OVA tumor–bearing mice ($P < 0.001$; Fig. 5C). The median survival time was longer than 150 days for the NP700-ARL(+) group, 70 days for the NP700 + Free ARL(+) group, 65 days for the NP700(+) group, and 41 days for the PBS group. NP700-ARL(+) outperformed NP700 + Free ARL(+) in this animal experiment, indicating that NP-based stimuli-response delivery of ARL is required for effective tumor response in vivo. To further test the elongation of survival, we kept monitoring the mice that received NP700-ARL(+) treatment for up to 300 days after tumor inoculation and found that six of eight mice survived over 300 days (fig. S15).

The therapeutic effect of NP700-ARL(+) was attributed to reprogramed tumor immune microenvironments in MC38 tumors. The NP700-ARL(+) treatment recruited more DCs in tumor sites as detected by flow cytometry (Fig. 5, D and E), promoted DC maturation with enhanced CD86 expression (fig. S16, A and B), and presented higher amounts of OVA peptide with MHC-I on the surface of DCs in both tumor sites and tumor-draining lymph nodes (TDLNs; Fig. 5F and fig. S16A). Although NP700(+) resulted in the accumulation of T_{regs}, the released ARL from NP700-ARL(+) reversed the increased T_{reg} ratio (Fig. 5, G and

H). Moreover, NP700-ARL(+) treatment induced a higher population of IFN-γ–producing $CD8^+$ T cells in tumor sites (Fig. 5, I and J). Examination of tumor-infiltrating antigen (OVA)–specific T cells also revealed that NP700-ARL(+) treatment induced expansion of OVA-specific $CD8^+$ T cells (fig. S16C). One week after light irradiation, we further observed an increase in systemic antigen-specific $CD8^+$ T cells in TDLNs and the spleen after NP700-ARL(+) treatment (Fig. 5K). To further examine whether the tumor antigen–specific T cell response was generated systemically, splenocytes from NP700-ARL(+)–treated mice were obtained and IFN-γ enzyme-linked immunospot (ELISpot) assay was performed in the presence of SIINFEKL peptide. The number of SIINFEKL-specific T cells increased in the NP700-ARL(+) group, indicating that this approach can induce tumor-specific T cell responses. We further isolated tumor-infiltrating $CD8^+$ T cells from MC38-OVA-Luc tumors and tested the cytotoxic effect ex vivo. As shown in Fig. 5 (M to O), tumor-infiltrating $CD8^+$ T cells isolated from NP700-ARL(+)–treated mice showed robust tumor-specific cell killing ability, with increased production of both IFN-γ and cytotoxic protease Granzyme B, supporting the hypothesis that $CD8^+$ T cells are responsible for the antitumor effects by NP700-ARL(+) treatment.

NP700-ARL(+) inhibits MOC1 tumor growth and stimulates anticancer immunity

We further evaluated tumor response to treatment with NPs in an orthotopic oral cancer model of MOC1 cells. We observed that NP700(+) partially suppressed tumor growth, whereas NP700-ARL(+) produced sustained tumor suppression (Fig. 6A). As shown in Fig. 6C, the mouse images on day 24 showed that the tumor was almost cured in the NP700-ARL(+) treatment group (five of eight mice were cured), leaving a small scar that was likely caused by the light treatment. In the long-term survival study, as presented in the Kaplan-Meier survival curves in Fig. 6B, the mice treated with NP700-ARL(+) survived significantly longer than other groups ($P < 0.001$, log-rank test). We used the change in body weight as an indicator of potential side effects. As shown in Fig. 6D, all treatments were safe for use in mice. Moreover, the surviving mice in the NP700-ARL(+) group resisted secondary tumor challenge (Fig. 6E), indicating that this approach triggered antitumor T cell memory in this model.

We investigated the change in the immune landscape in MOC1 tumors after ROS-responsive ARL delivery. The tumors were obtained from the mice 2 days after light irradiation and were analyzed by flow cytometry. Consistent with previous observations in the cell culture model, mechanistic studies revealed that NP700-ARL(+) activated DCs in the TME of MOC1 tumors, as evidenced by increased expression of CD86 on $CD11c^+$ DCs (fig. S17A). Moreover, NP700-ARL(+) increased the number of tumor-infiltrating $CD4^+$ and $CD8^+$ T cells in the TME (fig. S17B). As shown in Fig. 6F, NP700-ARL(+) significantly increased $CD8^+$ cell infiltration from 12.1 ± 2.7% to 20.5 ± 6.4% ($P < 0.05$). We also assayed the IFN-γ^+ $CD8^+$ T cell population in the tumor tissues. As shown in Fig. 6G, NP700-ARL(+) significantly increased the percentage of activated $CD8^+$ T cells in the TME, from 16.3 to 72.9% ($P < 0.001$). Furthermore, immunofluorescence images of MOC1 tumor tissues showed increased presence of $CD8^+$ and $CD69^+$ cells in the NP700-ARL(+)–treated tumors (fig. S18), which confirmed the results with flow cytometry. NP700(+)–treated tumors showed the lowest IFN-γ^+ $CD8^+$ T cell population (12.7%) although they had

sufficient DCs, which might be attributed to the increased CD39 and CD73 expression after NIR irradiation in the TME, including tumor cells, DCs, T cells, and myeloid-derived suppressor cells (MDSCs; fig. S19). Moreover, NP700(+) alone induced an increase in tumor-infiltrating $Foxp3^+CD4^+$ T_{regs} from 3.6 to 6.1%, whereas NP700-ARL(+) offsets the negative impact of PDT by significantly decreasing T_{reg} infiltration from 6.1%, induced by PDT, to 2.8%, which was similar to the PBS group ($P < 0.05$; Fig. 6H). To further evaluate the antitumor immunity of NP700-ARL(+), we studied the infiltration ratio of immune activator $CD8^+$ T cells and immune suppressor T_{regs} (Fig. 6I), and the results showed a significant increase in the $CD8^+/T_{reg}$ ratio of 7.7 for the NP700-ARL(+) group, whereas it was 3.8 for the PBS group and only 1.3 for the NP700(+) group [$P < 0.01$ with the PBS group, and $P < 0.001$ with the NP700(+) group].

Lymph nodes (LNs) are the site of immune regulation and optimal interactions between DCs that migrated from the tumor site, and effector T cells in the LNs facilitate adaptive immune responses that eliminate tumor cells (50). We detected increased $MHC\text{-}II^+CD86^+$ DCs in the draining LNs of the mice treated with NP700-ARL(+) (fig. S20). Moreover, the T_{reg} population in this group was significantly lower than that in the NP700(+) group (6.1 ± 1.5% versus 13.9 ± 1.2%; $P < 0.001$), indicating that the negative impact of T_{reg} induction by PDT was offset by ARL delivery (Fig. 6J). T_{regs} functionally impair $CD8^+$ T cells; thus, the NP700-ARL(+) treatment promoted cytotoxic $CD8^+$ T cell proliferation in the LNs, causing nearly 1.45-fold increase over the PBS group ($P < 0.01$; Fig. 6L). Furthermore, as shown in Fig. 6K, the activated IFN-γ^+ $CD8^+$ T cells in the NP700-ARL(+) group was significantly higher than that in the control groups ($P < 0.001$). As a result, NP700-ARL(+) significantly increased the $CD8^+/T_{reg}$ ratio in the draining LN being 5.1 for the PBS group, 2.7 for the NP700(+) group, and 7.4 for the NP700-ARL(+) group ($P < 0.01$ with the PBS group, and $P < 0.001$ with the NP700(+) group; Fig. 6M).

To evaluate the immunological memory responses induced by this approach, memory $CD8^+$ T cells were detected at day 35 by flow cytometry (Fig. 6N). The mice in the NP700-ARL(+) group showed significantly higher central memory T cells (T_{CM}; $CD62L^+CD44^+$) and effector memory T cells (T_{EM}; $CD62L^-CD44^+$) when compared with other groups ($P < 0.05$). Combined with the results from the rechallenging experiment in Fig. 6E, these results indicated that memory T cells were effectively reactivated. We further explored the abscopal effect of NP700-ARL–mediated PDT by distant tumor assay (Fig. 6O). We found that NP700-ARL(+) elicited robust therapeutic efficacy in combating not only primary tumor progression but also distant tumor growth, whereas NP700(+) treatment only induced tumor regression in irradiated primary tumors (Fig. 6P). These results suggested that NP700-ARL(+) treatment facilitates systemic antitumor immunity.

MOC1 and MOC2 tumors are carcinogen-induced and HPV-negative oral cancer tumors (51). Compared to MOC1, MOC2 tumors demonstrate aggressive and metastatic patterns and are less immunogenic because of low MHC I expression and high T_{reg} infiltration (48, 52), providing a more challenging model to test this approach. As shown in fig. S21A, MOC2 tumor growth was suppressed by the NP700-ARL(+) treatment. However, the tumor regression did not appear to be complete, as four of eight tumors regrew from day 30. We observed programmed death-ligand 1 (PD-L1) induction in MOC2 tumors

after the NP700-ARL(+) treatment (fig. S22), and the combination of this approach with anti-PD1 antibody achieved synergistic anticancer actions, leading to tumor regression (fig. S21B). Furthermore, the S1P receptor inhibitor FTY720, which prevents T cell egression from tumor-draining LNs (53), diminished the anticancer response by NP700-ARL(+) (fig. S21C), indicating that the recruitment of T cell from tumor-draining LNs is a critical step to induce antitumor immunity by this approach.

NP700-ARL(+) suppresses 4T1 tumor growth and reduces metastasis lesions in lung

We further extended our approach to a 4T1 orthotopic breast cancer model. As shown in Fig. 7 (A to C), NP700-ARL(+) outperformed NP700(+) or NP700-ARL in antitumor response in the 4T1 tumor model, leading to significantly longer median survival time of the tumor-bearing mice, from 24.5 days for the PBS group to 50 days for the NP700-ARL(+) group ($P < 0.001$). In addition, tumoral DCs in the NP700-ARL(+) group showed the highest expression of CD86 (Fig. 7D), indicating increased DC activation. The presence of tumor-infiltrating IFN-γ^+ $CD8^+$ T cells was the highest in the NP700-ARL(+) group (Fig. 7E), whereas that of T_{regs} was similar to the PBS group (Fig. 7F), resulting in the highest ratio of tumoral $CD8^+$ T cells/T_{regs} in the NP700-ARL(+) group (Fig. 7G). The multiplex immunofluorescence images of tumor tissues in fig. S23 further confirmed the flow cytometry results. To better discern the role of T cells, we performed $CD8^+$ and $CD4^+$ T cell depletion studies. As shown in Fig. 7H, $CD8^+$ T cell depletion reduced antitumor response to NP700-ARL(+), supporting the involvement of $CD8^+$ T cells. On the other hand, $CD4^+$ depletion resulted in modest reduction of anticancer response, likely due to the fact that $CD4^+$ effector and T_{regs} coexist in this cell population.

The 4T1 breast cancer model is highly metastatic. To evaluate the lung metastasis after different treatments, we removed primary 4T1-Luc tumors 3 weeks after tumor inoculation and monitored the mice for development of lung metastases by bioluminescence imaging on days 5 and 25 after surgery (Fig. 7I). Although mice in the PBS and NP700(+) groups developed lung metastases, none of the mice in the NP700-ARL(+) treatment group (zero of four) had any observed bioluminescence signal, indicating that formation of lung metastasis was inhibited by NP700-ARL(+) treatment. Metastasis foci in lungs were further examined by hematoxylin and eosin (H&E) staining 25 days after surgery, and the images in Fig. 7J confirmed the IVIS results, indicating that NP700-ARL(+) prevented formation of lung metastases of 4T1 tumors. When compared with MC38 and MOC1 models, although NP700-ARL(+) significantly inhibited 4T1 tumor growth ($P < 0.001$) and prolonged the survival of the mice ($P < 0.001$, log-rank test), it could not prevent the relapse of 4T1 tumors after day 25, with eight of eight mice being dead on day 70 (Fig. 7C). Furthermore, we observed elevated expression of PD-L1 on tumor cells after NP700-ARL(+) treatment by flow cytometry (Fig. 7K and fig. S24) and immunohistochemical (IHC) staining (fig. S25). The up-regulation of PD-L1 might have compromised the therapeutic outcome of NP700-ARL(+).We further combined anti-PD1 antibody therapy with NP700-ARL(+). Tumor regression was achieved through this combination therapy (Fig. 7L and fig. S26) and significantly prolonged survival of mice with a median survival time in excess of 100 days ($P < 0.001$, log-rank test; Fig. 7M). The mice cured with this combination approach generated long-term antitumor responses, showing a survival rate of 100% 58 days after

tumor rechallenge (Fig. 7N and fig. S27). To further study the observed prolonged survival, we continued to monitor the rechallenged mice receiving NP700-ARL(+) treatment, and 80% of them (n = 4) were cured, showing no signs of disease for at least 260 days after tumor rechallenge (fig. S28).

Immunological effects of NP700-ARL(+) in a patient-derived tumor spheroid model

According to the Human Protein Atlas dataset (54, 55), CD39 and CD73 are expressed in most human cancer tissues, including colon cancer, head and neck cancer, and breast cancer tissues, and the majority of them show moderate to strong expression (fig. S12). We examined the expression of CD39 and CD73 in human breast cancer and colon cancer tumor specimens by flow cytometry (fig. S13) and found that CD39 and CD73 were widely expressed in human TME. This indicated that the eATP might undergo quick degradation, which was already confirmed by the ATP hydrolysis experiment in Fig. 3D. We further assessed the therapeutic response of NP700-ARL(+) in human breast cancer tumors by establishing a patient-derived organotypic tumor spheroid (PDOTS) model. As shown in fig. S29A, the NP700(+) and NP700-ARL(+) treatments induced tumor cell death. Each treated group of the PDOTS was further incubated with human T cells that were isolated from two different donors. In fig. S29B, we observed that the T cell proliferation was suppressed in the NP700(+)–treated group, which might be due to ATP hydrolysis and Ado production after light irradiation (fig. S8), whereas NP700-ARL(+) reversed the immunosuppression caused by PDT and recovered T cell proliferation rate, thus promoting antitumor immunity. This suggests that our approach may have translational potential as a therapy for human cancer.

DISCUSSION

The observed clinical response rate of ICI monotherapy is about 20% across a variety of different cancer types (56). Moreover, ICIs can cause moderate to severe toxicities that require meaningful interventions, often resulting in ICI therapy interruption or discontinuation (56). Thus, approaches targeting other immune checkpoints are being investigated to increase the objective response rates to ICIs and to limit off-target toxicity (57). In the TME, eATP acts as a danger signal, playing a role in the recruitment of innate immune cells and in the priming of antitumor immunity (18, 22-25). Various cancer treatments can induce ATP release at high concentrations (17-21). However, eATP is quickly degraded into immunosuppressive Ado by the concerted enzymatic activity of ectonucleotidases CD39 and CD73, which are widely expressed in the TME, acting as a negative-feedback mechanism to prevent antitumor immunity (26, 28). There is thus a need to promote immunogenic TME, arrest tumor immunosuppressive activities, and avoid side effects for safe and effective cancer immunotherapy (6, 13).

In this study, we developed a combination therapy approach that, on the one hand, induces immunogenic cell death including ATP release, and, on the other hand, limits ATP degradation into Ado, thereby inducing durable antitumor immunity (fig. S30). We constructed ROS-responsive NPs carrying the CD39/CD73 inhibitor ARL and photosensitizer IR700. Upon light irradiation, the IR700-mediated PDT damaged cancer

cells, induced immunogenic cell death, and triggered the release of ATP. In conjunction, irradiation-generated ROS caused charge reversal of the NPs, which allowed responsive release of ARL and prevented conversion of eATP to Ado. We revealed that our approach could successfully induce immunogenic cell death in both patient-derived tumor cells and mouse tumor cells as indicated by increased production of eATP, HMGB1, and CRT, leading to increased DC maturation and cross-presentation of tumor antigens to prime and activate T cells. In a mouse model of oral cancer, NPs could successfully deliver IR700 and ARL to the tumor site, and upon light irradiation, tumor cells were quickly killed. The immunogenic TME was created with an increased $CD8^+/T_{reg}$ ratio that led to systemic and long-term tumor response in MOC1, MOC2, MC38, and 4T1 tumor models. In addition, in these models, we demonstrated that our approach could induce tumor-specific T cell responses and could elicit stronger antitumor response when combined with PD1 blockade. Moreover, in PDOTS models, NP700-ARL(+) not only induced light toxicity to tumor cells but also reversed the immunosuppression caused by PDT through recovering T cell proliferative responsiveness, thus promoting antitumor immunity. These results suggested that this approach might have translational potential as a therapy for human cancer.

ATP release from dying cancer cells is a common feature caused by various cancer treatments, and thus, conventional cancer treatments can generate anticancer immunity through inducing immunogenic cell death (17). However, this process is limited by Ado-mediated immunosuppressive mechanisms in the TME (58). Most cancer tissues display moderate to strong expression of CD39 and CD73 (54, 55), indicating that eATP can be degraded into Ado quickly after being released in the TME. In addition, CD39 and CD73 are expressed widely in various immune cell subsets (59-61). Recent studies have shown that CD39 is a marker of T cell activation and exhaustion (62, 63). Multiple regulatory mechanisms lie in immune activation to prevent the “overheat” immune response. The up-regulation of CD39 in activated $CD8^+$ or $CD4^+$ T cells is more likely an attempt to regulate excessive immune activation by their intrinsic capacity to provide stimulated T cells with a suppression function (64). In addition, CD39 is also highly expressed on immunosuppressive immune cells, such as T_{regs} and MDSCs, and the blockade of CD39 in these cells has shown impaired suppressive properties that would further restore effector T cell function (60, 65). Various previous studies also have shown that inhibition of CD39 enhances T cell activation instead of blocking the function of T cells (66-68), and therefore, CD39 was generally considered as an immune checkpoint molecular whose inhibition leads to the recovery of antitumor immunity (69).

AdoR antagonists are one class of small molecules that block adenosine 2a or adenosine 2b receptors and reactivate T cell–mediated antitumor immune response (35). Some of these antagonists showed early promise in clinical trials when combined with chemotherapy agents for the treatment of colorectal cancer, lung cancer, and breast cancer (70-73), indicating the translational potential of the approaches to target Ado signaling. When compared with the AdoR antagonists, our approach offers several advantages. Immune-modulating agents are intended to overcome these counter regulatory mechanisms and to unleash full potential of anticancer immunity by conventional cancer therapy. For this purpose, NP-based codelivery of conventional therapeutic agents with immune boosting agents can lead to synergistic combination therapy that is superior to monotherapy

or sequential administration of these agents. The codelivery system can improve drug accumulation at the tumor site, leading to durable anticancer immunity and long-term antitumor response. In addition, compared with AdoR antagonists that only block AdoR signaling, our approach not only reduces Ado-mediated immunosuppression but also induces immunogenic cell death and increases ATP-mediated immune stimulation. This dual functionality facilitates DC maturation and cross-presentation of tumor-specific antigens, thus likely leading to stronger T cell response and antitumor effects. Last, our NP-based codelivery system can lead to a safe cancer therapy, as the stimuli-responsive drug delivery allows for the ectonucleotidase inhibitor to be released when light irradiates at the tumor site, reducing potential systemic toxicity.

Several limitations exist within our current study. First, PDT is not a widely available cancer modality (74), which may be a hurdle for clinical translation of our NP approach. Second, our BA-based delivery system is only capable of delivering nucleotide drugs and could not encapsulate either chemotherapy agents or radiosensitizers at its current stage. Therefore, engineering the delivery system for combination with radiotherapy or chemotherapy will be the object of our future studies. In addition, although we demonstrated the NPs increased the drug delivery of ARL to MOC1 tumors and modulated the TME in different tumor models, it is still unclear how ATP and its metabolites play their discrete roles in regulating anticancer immunity in vivo. It is necessary to further investigate the mechanism and elucidate the interplay between them. Last, we validated our delivery system in a patient-derived tumor spheroid model, which is an in vitro model and is another limitation of our study. To further evaluate potential translation of our NP approach for treating human cancers, we will need to test it in a patient-derived xenograft humanized mouse model.

In conclusion, this study demonstrates the feasibility of using BA-based ROS-responsive NPs as a codelivery system to achieve both effective tumor ablation and a durable antitumor immune response. Considering the wide presence and the clinical impact of purinergic signaling in inflammation-related diseases (75, 76), this study is expected to have broad translational significance for the development of purinergic signaling-related therapeutics.

MATERIALS AND METHODS

Study design

The overall objective of this study was to develop a ROS-responsive NP to deliver an ectonucleotidase inhibitor to tumor sites and remodel the TME by overcoming Ado-mediated immunosuppression. For in vitro experiments, ATP hydrolysis, Ado production, DC maturation, T cell proliferation, and other experiments were performed at least three times independently. To establish our PDOTS model, human breast cancer or colon cancer tumor surgical specimens were obtained from the Tumor Tissue and Pathology Shared Resource at the Wake Forest Baptist Comprehensive Cancer Center using institutional review board–approved protocol (protocol no. IRB00073804) all patients provided written informed consent. We isolated T cells from the peripheral blood mononuclear cells (PBMCs) of healthy donors (HumanCells Biosciences) and cocultured them with PDOTS to study the effect on T cell proliferation. The number of samples for each experiment is listed in the figure legends, and the characteristics of healthy PBMC donors are listed in table S1.

For in vivo studies, experiments were all performed by using 4- to 8-week-old C57bl/6 mice or Babl/c mice. Mice were randomized to each group without blinding before treatment. The tumor accumulation of NPs was evaluated by IVIS experiment in MOC1-bearing C57bl/6 mice (n = 3 mice per group). The antitumor efficacy of NPs with or without αPD1 was evaluated in MC38-OVA–bearing C57bl/6 mice (n = 8 mice per group), MOC-bearing C57bl/6 mice (n = 8 mice per group), or 4T1-bearing Babl/c mice (n = 8 mice per group). Luciferase-expressing cell lines were used for in vivo imaging to monitor tumor growth or metastatic burden. The rechallenge experiment was evaluated in MOC-bearing C57bl/6 mice (n = 6 mice per group) or 4T1-bearing Babl/c mice (n = 5 or 6 mice per group). Mice were monitored daily and euthanized at defined humane end points. The tumor samples from these studies are also used to study the immune cell populations by flow cytometry, immunofluorescence staining, IHC staining, or other assays. Blinding was not done except for the IHC staining and ELISA assay. All animal experiments were done according to a protocol approved by the Wake Forest Institutional Animal Care and Use Committee.

Cell lines

Murine oral cancer (MOC1 and MOC2) cells were provided by R. Uppaluri (Harvard University School of Medicine) and were cultured in HyClone Iscove's Modified Dulbecco's Medium (GE Healthcare Life sciences)/HyClone Ham's Nutrient Mixture F12 (GE Healthcare Life Sciences) at a 2:1 mixture with 5% fetal bovine serum (FBS; Life Technologies), 1% penicillin/streptomycin (Life Technologies), epidermal growth factor (5 ng/ml; EMD Millipore Corporation), hydrocortisone (400 ng/ml; Sigma Aldrich), and insulin (5 mg/ml; Sigma Aldrich). The mouse breast cancer cells 4T1 (provided by Y. Shiozawa, Wake Forest University School of Medicine), the OVA-transfected mouse colon cancer cells MC38-OVA (provided by Y. Lu, Wake Forest University School of Medicine), the 4T1 cells, or MC38-OVA cells stably transfected with firefly luciferase (4T1-Luc, MC38-OVA-Luc) were cultured in Dulbecco's modified Eagle's medium, supplemented with 10% FBS, penicillin (100 U/ml), and streptomycin (100 μg/ml). All cell lines were maintained in a humidified atmosphere containing 5% CO_2 at 37°C.

NP preparation

DSPE-PEG_{2000}-NH_2 and PDEAEA-PBA were purchased from Nanosoft Polymers LLC, and IR700-NHS was purchased from LI-COR Biosciences. The structure of PDEAEA-PBA was confirmed by proton nuclear magnetic resonance (^{1}H NMR): δ 7.2 to 8.0 (4H, ArH), δ 4.0 to 4.6 (4H, $ArCH_2N$, $COOCH_2$), δ 3.0 to 3.6 [6H, $N(CH_2CH_3)_2CH_2CH_2OOC$], δ 2.3 to 2.6 (1H, CH_2CH), and δ 0.8 to 1.6 [8H, $N(CH_2CH_3)_2$, CH_2CH]. UTP^{AF546} was from Thermo Fisher Scientific. To prepare NP700-ARL, the DSPE-PEG_{2000}-NH_2 was reacted with IR700-NHS in methanol at a ratio of 1:1 to produce DSPE-PEG_{2000}-IR700. Then, DSPE-PEG_{2000}/DSPE-PEG_{2000}-IR700 and PDEAEA-PBA were mixed in methanol at a ratio of 1:10 and added into Hepes buffer containing nucleotides under sonication. Methanol and free nucleotides molecular were removed by ultrafiltration, and the loaded nucleotides were calculated by subtraction of the nucleotides in filtrate detected by ultraviolet absorbance. The nucleotide binding ability of the NP700 was evaluated by agarose gel retardation assay. The polyplexes of NP700-UTP^{AF546} were electrophoresed on a 1.5% agarose gel at 100 V for 10 min. The size and zeta potential of the NP700-ARL were

measured at 25°C using a Zetasizer Nano-ZS. Data are presented as the means ± SD ($n = 3$). The morphology of the NPs was stained with water-soluble phosphotungstic acid (PTA) and was visualized using a transmission electron microscope (TEM; JEM-1200EX).

DC maturation experiment

DCs were generated from the 6-week-old C57bl/6 female mice using a method previously reported (77). Briefly, mouse bone marrow (BM) cells were collected through flushing the tibia and femur with AIM V medium (Gibco). Subsequently, the cells were cultured in AIM V medium, penicillin/streptomycin, granulocyte-macrophage colony-stimulating factor (20 ng/ml), IL-4 (5 ng/ml), and 1× 2-mercaptoethanol. Half of the culture medium was replaced every other day, and the nonadherent and loosely adherent cells were collected on day 8 and phenotyped for immature DCs by measuring CD11c expression (typically over 80% $CD11c^+$).

Immature BM-derived DCs (BMDC) were coincubated with MOC1 cells that had undergone the NP treatment and light irradiation. After 24 hours, DCs were stained with anti-mouse CD45, anti-mouse MHC-II, and anti-mouse CD86 antibodies (eBioscience) and analyzed by flow cytometry.

OT-I cell stimulation by dendritic cells

Immature DCs were coincubated with MOC1-OVA cells that had been treated in different groups. After 24 hours, $OVA_{257–264}$ that was presented with MHC-I on the cell surface was detected by anti-H-$2K^b$ bound to SIINFEKL, an antibody that specifically recognizes OVA peptide SIINFEKL bound to H-$2K^b$ of MHC-I.

Naïve $CD8^+$ T cells (OT-I cells) were isolated from C57BL/6-Tg(TcraTcrb)1100Mjb/J mice spleens with a naïve $CD8^+$ T cell isolation kit (Miltenyi Biotec). These responder cells (2×10^4) were further cultured with the mixture of DCs and MOC1-OVA cells (1×10^4) in round-bottom 96-well plates. Supernatants were collected after 48 hours and assayed for IFN-γ by ELISA (Thermo Fisher Scientific).

Animals

All animal experiments were done according to a protocol approved by the Wake Forest Institutional Animal Care and Use Committee. C57BL/6-Tg(TcraTcrb)1100Mjb/J mice, C57bl/6 mice (4 to 6 weeks old), and Balb/c mice (6 to 8 weeks old) were purchased from the Jackson Laboratory (Bar Harbor, ME, USA) for animal studies.

In vivo phototherapy in different tumor models

To establish oral cancer models, 1×10^6 MOC1 cells or 2×10^6 MOC2 cells were injected into the floor of the mouth of C57bl/6 mice by an extra-oral approach. To establish orthotropic breast cancer models, 5×10^5 4T1-Luc cells were injected into the right second mammary fat pad of female Balb/c mice. To establish substances of colon cancer models, 2×10^6 MC38-OVA-Luc or MC38-OVA cells were subcutaneously injected into the right flank of C57bl/6 mice. After 12 days for the MOC1 model and 14 days for the MC38 model, mice were randomly allocated into five groups ($n = 8$): PBS, NP700-ARL, NP700(+),

NP700-ARL(+), and NP700 + Free ARL(+), and received intravenous injection of PBS, NP700-ARL, NP700, NP700-ARL, NP700 plus free ARL (12 mg/kg of ARL and 0.5 mg/kg of IR700) on days 12 and 15 for the MOC1 model and days 14 and 17 for the MC38 model, respectively. For the 4T1 model, after 10 days of tumor inoculation, mice were randomly allocated into six groups ($n = 8$): PBS, NP700-ARL, NP700(+), NP700-ARL(+), NP700(+) plus αPD1, and NP700-ARL(+) plus αPD1, and received intravenous injection of PBS, NP700-ARL, NP700, NP700-ARL, NP700, and NP700-ARL on days 10 and 13, respectively. The tumor sites in (+) marked groups were exposed to the 690-nm light-emitting diode (LED) light at a total dose of 50 J/cm^2 4 hours after injection. Anti-PD1 antibody was injected intraperitoneally for a dose of 10 mg/kg at 1, 4, 7, and 10 days after light irradiation. For the MOC2 tumor model, after 7 days of tumor inoculation, mice were randomly allocated into seven groups ($n = 8$): PBS, NP700-ARL, NP700(+), NP700-ARL(+), NP700(+) + αPD1, NP700-ARL(+) + αPD1, and NP700-ARL(+) + FTY720. FTY720 was given intraperitoneally at a dose of 3 mg/kg starting on day 6 and continuing twice weekly. Mice were euthanized by carbon dioxide inhalation when any tumor size was larger than 800 mm^3 for the MC38 model and 1000 mm^3 for the other models.

For lung metastases observation, 4T1-Luc cells were inoculated to the fat pad of Balb/c mice and treated in different groups as described above ($n = 4$). Primary tumor was surgically removed 21 days after tumor inoculation. The lung metastasis of 4T1 tumor was monitored by in vivo bioluminescence imaging and confirmed by ex vivo examination and H&E staining.

For the abscopal effect experiment, primary MOC1 tumor cells (1×10^6) were inoculated at the left flank of C57bl/6 mice at day 0, and the distant tumor (3×10^5) was inoculated at the right flank of the same mouse at day 8, mice were treated in different groups as described above on days 12 and 15.

Statistical analysis

Quantitative data were expressed as means ± SD. Means were compared using one-way analysis of variance (ANOVA) or two-way ANOVA for multiple comparisons. *P* values smaller than 0.05 were considered statistically significant. Survival analysis was conducted with Kaplan-Meier curves, and their comparison was determined by log-rank (Mantel-Cox) test.

Supplementary Material

Refer to Web version on PubMed Central for supplementary material.

Acknowledgments:

We thank R. Uppaluri (Harvard University) for providing murine oral cancer MOC1 and MOC2 cells, Y. Shiozawa (Wake Forest University) for providing murine breast cancer 4T1 cells, and Y. Lu (Wake Forest University) for providing the OVA-transfected mouse colon cancer MC38-OVA cells.

Funding:

We would like to acknowledge the supports by the NIH grants R01CA194064, R21CA267853, and R21CA263759 to X.M. This work was also supported by a pilot grant to X.M. from the Wake Forest Baptist Comprehensive

Cancer Center, supported by the NCI's Cancer Center Support Grant P30CA012197, and a pilot grant to X.M. from the Wake Forest Clinical and Translational Science Institute, supported by a Clinical and Translational Science Award from the NIH through Grant Award Number UL1TR001420.

REFERENCES AND NOTES

1. Sanmamed MF, Chen L, A paradigm shift in cancer immunotherapy: From enhancement to normalization. Cell 175, 313–326 (2018). [PubMed: 30290139]
2. Patsoukis N, Wang Q, Strauss L, Boussiotis VA, Revisiting the PD-1 pathway. Sci. Adv 6, eabd2712 (2020). [PubMed: 32948597]
3. Sharma P, Hu-Lieskovan S, Wargo JA, Ribas A, Primary, adaptive, and acquired resistance to cancer immunotherapy. Cell 168, 707–723 (2017). [PubMed: 28187290]
4. Togashi Y, Shitara K, Nishikawa H, Regulatory T cells in cancer immunosuppression - Implications for anticancer therapy. Nat. Rev. Clin. Oncol 16, 356–371 (2019). [PubMed: 30705439]
5. Christmas BJ, Rafie CI, Hopkins AC, Scott BA, Ma HS, Cruz KA, Woolman S, Armstrong TD, Connolly RM, Azad NA, Jaffee EM, Roussos Torres ET, Entinostat converts immune-resistant breast and pancreatic cancers into checkpoint-responsive tumors by reprogramming tumor-infiltrating MDSCs. Cancer Immunol. Res 6, 1561–1577 (2018). [PubMed: 30341213]
6. Sharma P, Allison JP, The future of immune checkpoint therapy. Science 348, 56–61 (2015). [PubMed: 25838373]
7. Dogan V, Rieckmann T, Munscher A, Busch CJ, Current studies of immunotherapy in head and neck cancer. Clin. Otolaryngol 43, 13–21 (2018). [PubMed: 28464441]
8. Solinas C, Gombos A, Latifyan S, Piccart-Gebhart M, Kok M, Buisseret L, Targeting immune checkpoints in breast cancer: An update of early results. ESMO Open 2, e000255 (2017). [PubMed: 29177095]
9. Young A, Ngiow SF, Barkauskas DS, Sult E, Hay C, Blake SJ, Huang Q, Liu J, Takeda K, Teng MWL, Sachsenmeier K, Smyth MJ, Co-inhibition of CD73 and A2AR adenosine signaling improves anti-tumor immune responses. Cancer Cell 30, 391–403 (2016). [PubMed: 27622332]
10. Seiwert TY, Burtness B, Mehra R, Weiss J, Berger R, Eder JP, Heath K, McClanahan T, Lunceford J, Gause C, Cheng JD, Chow LQ, Safety and clinical activity of pembrolizumab for treatment of recurrent or metastatic squamous cell carcinoma of the head and neck (KEYNOTE-012): An open-label, multicentre, phase 1b trial. Lancet Oncol. 17, 956–965 (2016). [PubMed: 27247226]
11. Plitas G, Rudensky AY, Regulatory T cells: Differentiation and function. Cancer Immunol. Res 4, 721–725 (2016). [PubMed: 27590281]
12. Munn DH, Bronte V, Immune suppressive mechanisms in the tumor microenvironment. Curr. Opin. Immunol 39, 1–6 (2016). [PubMed: 26609943]
13. Moynihan KD, Opel CF, Szeto GL, Tzeng A, Zhu EF, Engreitz JM, Williams RT, Rakhra K, Zhang MH, Rothschilds AM, Kumari S, Kelly RL, Kwan BH, Abraham W, Hu K, Mehta NK, Kauke MJ, Suh H, Cochran JR, Lauffenburger DA, Wittrup KD, Irvine DJ, Eradication of large established tumors in mice by combination immunotherapy that engages innate and adaptive immune responses. Nat. Med 22, 1402–1410 (2016). [PubMed: 27775706]
14. Cekic C, Linden J, Purinergic regulation of the immune system. Nat. Rev. Immunol 16, 177–192 (2016). [PubMed: 26922909]
15. Gorini S, la Sala A, Hydrolysis of extracellular ATP and immune suppression: Humans versus mice. Blood 111, 964–965 (2008). [PubMed: 18182581]
16. Blay J, White TD, Hoskin DW, The extracellular fluid of solid carcinomas contains immunosuppressive concentrations of adenosine. Cancer Res. 57, 2602–2605 (1997). [PubMed: 9205063]
17. Kroemer G, Galluzzi L, Kepp O, Zitvogel L, Immunogenic cell death in cancer therapy. Annu. Rev. Immunol 31, 51–72 (2013). [PubMed: 23157435]
18. Ghiringhelli F, Apetoh L, Tesniere A, Aymeric L, Ma Y, Ortiz C, Vermaelen K, Panaretakis T, Mignot G, Ullrich E, Perfettini JL, Schlemmer F, Tasdemir E, Uhl M, Genin P, Civas A, Ryffel B, Kanellopoulos J, Tschopp J, Andre F, Lidereau R, McLaughlin NM, Haynes NM, Smyth MJ, Kroemer G, Zitvogel L, Activation of the NLRP3 inflammasome in dendritic cells

induces IL-1beta-dependent adaptive immunity against tumors. Nat. Med 15, 1170–1178 (2009). [PubMed: 19767732]

19. Hoorelbeke D, Decrock E, De Smet M, De Bock M, Descamps B, Van Haver V, Delvaeye T, Krysko DV, Vanhove C, Bultynck G, Leybaert L, Cx43 channels and signaling via IP3/$Ca2^{+}$, ATP, and ROS/NO propagate radiation-induced DNA damage to non-irradiated brain microvascular endothelial cells. Cell Death Dis. 11, 194 (2020). [PubMed: 32188841]
20. Liu H, Hu Y, Sun Y, Wan C, Zhang Z, Dai X, Lin Z, He Q, Yang Z, Huang P, Xiong Y, Cao J, Chen X, Chen Q, Lovell JF, Xu Z, Jin H, Yang K, Co-delivery of bee venom melittin and a photosensitizer with an organic-inorganic hybrid nanocarrier for photodynamic therapy and immunotherapy. ACS Nano 13, 12638–12652 (2019). [PubMed: 31625721]
21. Agne A, Richter K, Tumpara S, Sauer AL, Beckert F, Wrenger S, Zakrzewicz A, Hecker A, Markmann M, Koch C, Zajonz T, Sander M, Boning A, Padberg W, Janciauskiene S, Grau V, Does heart surgery change the capacity of α1-antitrypsin to inhibit the ATP-induced release of monocytic interleukin-1 β? A preliminary study. Int. Immunopharmacol 81, 106297 (2020). [PubMed: 32062078]
22. Michaud M, Martins I, Sukkurwala AQ, Adjemian S, Ma Y, Pellegatti P, Shen S, Kepp O, Scoazec M, Mignot G, Rello-Varona S, Tailler M, Menger L, Vacchelli E, Galluzzi L, Ghiringhelli F, di Virgilio F, Zitvogel L, Kroemer G, Autophagy-dependent anticancer immune responses induced by chemotherapeutic agents in mice. Science 334, 1573–1577 (2011). [PubMed: 22174255]
23. Aymeric L, Apetoh L, Ghiringhelli F, Tesniere A, Martins I, Kroemer G, Smyth MJ, Zitvogel L, Tumor cell death and ATP release prime dendritic cells and efficient anticancer immunity. Cancer Res. 70, 855–858 (2010). [PubMed: 20086177]
24. Elliott MR, Chekeni FB, Trampont PC, Lazarowski ER, Kadl A, Walk SF, Park D, Woodson RI, Ostankovich M, Sharma P, Lysiak JJ, Harden TK, Leitinger N, Ravichandran KS, Nucleotides released by apoptotic cells act as a find-me signal to promote phagocytic clearance. Nature 461, 282–286 (2009). [PubMed: 19741708]
25. Chen Y, Corriden R, Inoue Y, Yip L, Hashiguchi N, Zinkernagel A, Nizet V, Insel PA, Junger WG, ATP release guides neutrophil chemotaxis via P2Y2 and A3 receptors. Science 314, 1792–1795 (2006). [PubMed: 17170310]
26. Krysko DV, Garg AD, Kaczmarek A, Krysko O, Agostinis P, Vandenabeele P, Immunogenic cell death and DAMPs in cancer therapy. Nat. Rev. Cancer 12, 860–875 (2012). [PubMed: 23151605]
27. Galluzzi L, Buque A, Kepp O, Zitvogel L, Kroemer G, Immunogenic cell death in cancer and infectious disease. Nat. Rev. Immunol 17, 97–111 (2017). [PubMed: 27748397]
28. Allard B, Longhi MS, Robson SC, Stagg J, The ectonucleotidases CD39 and CD73: Novel checkpoint inhibitor targets. Immunol. Rev 276, 121–144 (2017). [PubMed: 28258700]
29. Ohta A, A metabolic immune checkpoint: Adenosine in tumor microenvironment. Front. Immunol 7, 109 (2016). [PubMed: 27066002]
30. Ohta A, Gorelik E, Prasad SJ, Ronchese F, Lukashev D, Wong MK, Huang X, Caldwell S, Liu K, Smith P, Chen JF, Jackson EK, Apasov S, Abrams S, Sitkovsky M, A2A adenosine receptor protects tumors from antitumor T cells. Proc. Natl. Acad. Sci. U.S.A 103, 13132–13137 (2006). [PubMed: 16916931]
31. Sitkovsky MV, Kjaergaard J, Lukashev D, Ohta A, Hypoxia-adenosinergic immunosuppression: Tumor protection by T regulatory cells and cancerous tissue hypoxia. Clin. Cancer Res 14, 5947–5952 (2008). [PubMed: 18829471]
32. Li XY, Moesta AK, Xiao C, Nakamura K, Casey M, Zhang H, Madore J, Lepletier A, Aguilera AR, Sundarrajan A, Jacoberger-Foissac C, Wong C, Dela Cruz T, Welch M, Lerner AG, Spatola BN, Soros VB, Corbin J, Anderson AC, Effern M, Holzel M, Robson SC, Johnston RL, Waddell N, Smith C, Bald T, Geetha N, Beers C, Teng MWL, Smyth MJ, Targeting CD39 in cancer reveals an extracellular ATP- and inflammasome-driven tumor immunity. Cancer Discov. 9, 1754–1773 (2019). [PubMed: 31699796]
33. Baghdadi M, Wada H, Nakanishi S, Abe H, Han N, Putra WE, Endo D, Watari H, Sakuragi N, Hida Y, Kaga K, Miyagi Y, Yokose T, Takano A, Daigo Y, Seino KI, Chemotherapy-induced IL34 enhances immunosuppression by tumor-associated macrophages and mediates survival of chemoresistant lung cancer cells. Cancer Res. 76, 6030–6042 (2016). [PubMed: 27550451]

34. Vijayan D, Young A, Teng MWL, Smyth MJ, Targeting immunosuppressive adenosine in cancer. Nat. Rev. Cancer 17, 709–724 (2017). [PubMed: 29059149]
35. Hou J, Greten TF, Xia Q, Immunosuppressive cell death in cancer. Nat. Rev. Immunol 17, 401 (2017).
36. Al-Rashida M, Qazi SU, Batool N, Hameed A, Iqbal J, Ectonucleotidase inhibitors: A patent review (2011-2016). Expert Opin. Ther. Pat 27, 1291–1304 (2017). [PubMed: 28870136]
37. Shapiro MJ, Jellinek M, Pyrros D, Sundine M, Baue AE, Clearance and maintenance of blood nucleotide levels with adenosine triphosphate-magnesium chloride injection. Circ. Shock 36, 62–67 (1992). [PubMed: 1551186]
38. Miyabe H, Hyodo M, Nakamura T, Sato Y, Hayakawa Y, Harashima H, A new adjuvant delivery system 'cyclic di-GMP/YSK05 liposome' for cancer immunotherapy. J. Control. Release 184, 20–27 (2014). [PubMed: 24727060]
39. Liu Y, Crowe WN, Wang L, Lu Y, Petty WJ, Habib AA, Zhao D, An inhalable nanoparticulate STING agonist synergizes with radiotherapy to confer long-term control of lung metastases. Nat. Commun 10, 5108 (2019). [PubMed: 31704921]
40. Vivian JP, Riedmaier P, Ge H, Le Nours J, Sansom FM, Wilce MC, Byres E, Dias M, Schmidberger JW, Cowan PJ, d'Apice AJ, Hartland EL, Rossjohn J, Beddoe T, Crystal structure of a Legionella pneumophila ecto - Triphosphate diphosphohydrolase, a structural and functional homolog of the eukaryotic NTPDases. Structure 18, 228–238 (2010). [PubMed: 20159467]
41. Gulfam M, Sahle FF, Lowe TL, Design strategies for chemical-stimuli-responsive programmable nanotherapeutics. Drug Discov. Today 24, 129–147 (2018). [PubMed: 30292916]
42. Antonio JPM, Russo R, Carvalho CP, Cal PMSD, Gois PMP, Boronic acids as building blocks for the construction of therapeutically useful bioconjugates. Chem. Soc. Rev 48, 3513–3536 (2019). [PubMed: 31157810]
43. Liu X, Xiang J, Zhu D, Jiang L, Zhou Z, Tang J, Liu X, Huang Y, Shen Y, Fusogenic reactive oxygen species triggered charge-reversal vector for effective gene delivery. Adv. Mater 28, 1743–1752 (2016). [PubMed: 26663349]
44. Wang L, Xie S, Ma L, Chen Y, Lu W, 10-Boronic acid substituted camptothecin as prodrug of SN-38. Eur. J. Med. Chem 116, 84–89 (2016). [PubMed: 27060760]
45. Kim EJ, Bhuniya S, Lee H, Kim HM, Cheong C, Maiti S, Hong KS, Kim JS, An activatable prodrug for the treatment of metastatic tumors. J. Am. Chem. Soc 136, 13888–13894 (2014). [PubMed: 25238144]
46. Schakel L, Schmies CC, Idris RM, Luo X, Lee SY, Lopez V, Mirza S, Vu TH, Pelletier J, Sevigny J, Namasivayam V, Muller CE, Nucleotide analog ARL67156 as a lead structure for the development of CD39 and dual CD39/CD73 ectonucleotidase inhibitors. Front. Pharmacol 11, 1294 (2020). [PubMed: 33013365]
47. Moore EC, Cash HA, Caruso AM, Uppaluri R, Hodge JW, Van Waes C, Allen CT, Enhanced tumor control with combination mTOR and PD-L1 inhibition in syngeneic oral cavity cancers. Cancer Immunol. Res 4, 611–620 (2016). [PubMed: 27076449]
48. Moore E, Clavijo PE, Davis R, Cash H, Van Waes C, Kim Y, Allen C, Established T cell-inflamed tumors rejected after adaptive resistance was reversed by combination STING activation and PD-1 pathway blockade. Cancer Immunol. Res 4, 1061–1071 (2016). [PubMed: 27821498]
49. Shirasu N, Nam SO, Kuroki M, Tumor-targeted photodynamic therapy. Anticancer Res 33, 2823–2831 (2013). [PubMed: 23780966]
50. Zheng R, Kjaergaard J, Lee WT, Cohen PA, Shu S, Significance of regional draining lymph nodes in the development of tumor immunity: Implications for cancer immunotherapy. Cancer Treat. Res 135, 223–237 (2007). [PubMed: 17953420]
51. Judd NP, Winkler AE, Murillo-Sauca O, Brotman JJ, Law JH, Lewis JS Jr., Dunn GP, Bui JD, Sunwoo JB, Uppaluri R, ERK1/2 regulation of CD44 modulates oral cancer aggressiveness. Cancer Res. 72, 365–374 (2012). [PubMed: 22086849]
52. Judd NP, Allen CT, Winkler AE, Uppaluri R, Comparative analysis of tumor-infiltrating lymphocytes in a syngeneic mouse model of oral cancer. Otolaryngol. Head Neck Surg 147, 493–500 (2012). [PubMed: 22434099]

53. Brinkmann V, Cyster JG, Hla T, FTY720: Sphingosine 1-phosphate receptor-1 in the control of lymphocyte egress and endothelial barrier function. Am. J. Transplant 4, 1019–1025 (2004). [PubMed: 15196057]
54. Uhlen M, Fagerberg L, Hallstrom BM, Lindskog C, Oksvold P, Mardinoglu A, Sivertsson A, Kampf C, Sjostedt E, Asplund A, Olsson I, Edlund K, Lundberg E, Navani S, Szigyarto CA, Odeberg J, Djureinovic D, Takanen JO, Hober S, Alm T, Edqvist PH, Berling H, Tegel H, Mulder J, Rockberg J, Nilsson P, Schwenk JM, Hamsten M, von Feilitzen K, Forsberg M, Persson L, Johansson F, Zwahlen M, von Heijne G, Nielsen J, Ponten F, Proteomics. Tissue-based map of the human proteome. Science 347, 1260419 (2015). [PubMed: 25613900]
55. Uhlen M, Zhang C, Lee S, Sjostedt E, Fagerberg L, Bidkhori G, Benfeitas R, Arif M, Liu Z, Edfors F, Sanli K, von Feilitzen K, Oksvold P, Lundberg E, Hober S, Nilsson P, Mattsson J, Schwenk JM, Brunnstrom H, Glimelius B, Sjoblom T, Edqvist PH, Djureinovic D, Micke P, Lindskog C, Mardinoglu A, Ponten F, A pathology atlas of the human cancer transcriptome. Science 357, eaan2507 (2017). [PubMed: 28818916]
56. Jenkins RW, Barbie DA, Flaherty KT, Mechanisms of resistance to immune checkpoint inhibitors. Br. J. Cancer 118, 9–16 (2018). [PubMed: 29319049]
57. Galluzzi L, Chan TA, Kroemer G, Wolchok JD, Lopez-Soto A, The hallmarks of successful anticancer immunotherapy. Sci. Transl. Med 10, eaat7807 (2018). [PubMed: 30232229]
58. Allard B, Beavis PA, Darcy PK, Stagg J, Immunosuppressive activities of adenosine in cancer. Curr. Opin. Pharmacol 29, 7–16 (2016). [PubMed: 27209048]
59. Shevchenko I, Mathes A, Groth C, Karakhanova S, Muller V, Utikal J, Werner J, Bazhin AV, Umansky V, Enhanced expression of CD39 and CD73 on T cells in the regulation of anti-tumor immune responses. Onco. Targets. Ther 9, 1744946 (2020).
60. Li L, Wang L, Li J, Fan Z, Yang L, Zhang Z, Zhang C, Yue D, Qin G, Zhang T, Li F, Chen X, Ping Y, Wang D, Gao Q, He Q, Huang L, Li H, Huang J, Zhao X, Xue W, Sun Z, Lu J, Yu JJ, Zhao J, Zhang B, Zhang Y, Metformin-induced reduction of CD39 and CD73 blocks myeloid-derived suppressor cell activity in patients with ovarian cancer. Cancer Res. 78, 1779–1791 (2018). [PubMed: 29374065]
61. Pulte ED, Broekman MJ, Olson KE, Drosopoulos JH, Kizer JR, Islam N, Marcus AJ, CD39/NTPDase-1 activity and expression in normal leukocytes. Thromb. Res 121, 309–317 (2007). [PubMed: 17555802]
62. Canale FP, Ramello MC, Nunez N, Araujo Furlan CL, Bossio SN, Gorosito Serran M, Tosello Boari J, Del Castillo A, Ledesma M, Sedlik C, Piaggio E, Gruppi A, Rodriguez EAA, Montes CL, CD39 expression defines cell exhaustion in tumor-infiltrating $CD8^+$ T cells. Cancer Res. 78, 115–128 (2018). [PubMed: 29066514]
63. Simoni Y, Becht E, Fehlings M, Loh CY, Koo SL, Teng KWW, Yeong JPS, Nahar R, Zhang T, Kared H, Duan K, Ang N, Poidinger M, Lee YY, Larbi A, Khng AJ, Tan E, Fu C, Mathew R, Teo M, Lim WT, Toh CK, Ong BH, Koh T, Hillmer AM, Takano A, Lim TKH, Tan EH, Zhai W, Tan DSW, Tan IB, Newell EW, Bystander $CD8^+$ T cells are abundant and phenotypically distinct in human tumour infiltrates. Nature 557, 575–579 (2018). [PubMed: 29769722]
64. Timperi E, Barnaba V, CD39 regulation and functions in T cells. Int. J. Mol. Sci 22, (2021).
65. Deaglio S, Dwyer KM, Gao W, Friedman D, Usheva A, Erat A, Chen JF, Enjyoji K, Linden J, Oukka M, Kuchroo VK, Strom TB, Robson SC, Adenosine generation catalyzed by CD39 and CD73 expressed on regulatory T cells mediates immune suppression. J. Exp. Med 204, 1257–1265 (2007). [PubMed: 17502665]
66. Bastid J, Regairaz A, Bonnefoy N, Dejou C, Giustiniani J, Laheurte C, Cochaud S, Laprevotte E, Funck-Brentano E, Hemon P, Gros L, Bec N, Larroque C, Alberici G, Bensussan A, Eliaou JF, Inhibition of CD39 enzymatic function at the surface of tumor cells alleviates their immunosuppressive activity. Cancer Immunol. Res 3, 254–265 (2015). [PubMed: 25403716]
67. Hausler SF, Montalban del Barrio I, Strohschein J, Chandran PA, Engel JB, Honig A, Ossadnik M, Horn E, Fischer B, Krockenberger M, Heuer S, Seida AA, Junker M, Kneitz H, Kloor D, Klotz KN, Dietl J, Wischhusen J, Ectonucleotidases CD39 and CD73 on OvCA cells are potent adenosine-generating enzymes responsible for adenosine receptor 2A-dependent suppression of T cell function and NK cell cytotoxicity. Cancer Immunol. Immunother CII 60, 1405–1418 (2011).

68. Xue G, Zheng N, Fang J, Jin G, Li X, Dotti G, Yi Q, Lu Y, Adoptive cell therapy with tumor-specific Th9 cells induces viral mimicry to eliminate antigen-loss-variant tumor cells. Cancer Cell 39, 1610–1622.e9 (2021). [PubMed: 34678150]
69. Allard D, Allard B, Stagg J, On the mechanism of anti-CD39 immune checkpoint therapy. J. Immunother. Cancer 8, e000186 (2020). [PubMed: 32098829]
70. Chiappori A, Williams CC, Creelan BC, Tanvetyanon T, Gray JE, Haura EB, Thapa R, Chen D-T, Beg AA, Boyle TA, Bendiske J, Morris E, Tao A, Hurtado FK, Manenti L, Castro J, Antonia SJ, Phase I/II study of the A2AR antagonist NIR178 (PBF-509), an oral immunotherapy, in patients (pts) with advanced NSCLC. J. Clin. Oncol 36, 9089 (2018).
71. Lim EA, Bauer TM, Patel MR, Falchook GS, Karlix JL, Choe JH, George DJ, Mugundu GM, Pilling E, Chen H, Linghu B, McGrath L, Shao W, Merchant MS, Sidders B, Sachsenmeier KF, Pouliot GP, Drake CG, Bendell JC, A phase I, open-label, multicenter study to assess the safety, pharmacokinetics, and preliminary antitumor activity of AZD4635 both as monotherapy and in combination in patients with advanced solid malignancies: Results from prostate cancer patients (NCT02740985). J. Clin. Oncol 38, 5518 (2020).
72. Cecchini M, Krishnan K, Giafis N, Scott J, Quah CS, Bendell JC, ARC-9: Phase Ib/II study to evaluate etrumadenant (AB928)-based treatment combinations in patients with metastatic colorectal cancer (mCRC). J. Clin. Oncol 39, TPS150 (2021).
73. Fong L, Hotson A, Powderly JD, Sznol M, Heist RS, Choueiri TK, George S, Hughes BGM, Hellmann MD, Shepard DR, Rini BI, Kummar S, Weise AM, Riese MJ, Markman B, Emens LA, Mahadevan D, Luke JJ, Laport G, Brody JD, Hernandez-Aya L, Bonomi P, Goldman JW, Berim L, Renouf DJ, Goodwin RA, Munneke B, Ho PY, Hsieh J, McCaffery I, Kwei L, Willingham SB, Miller RA, Adenosine 2A receptor blockade as an immunotherapy for treatment-refractory renal cell cancer. Cancer Discov. 10, 40–53 (2020). [PubMed: 31732494]
74. Agostinis P, Berg K, Cengel KA, Foster TH, Girotti AW, Gollnick SO, Hahn SM, Hamblin MR, Juzeniene A, Kessel D, Korbelik M, Moan J, Mroz P, Nowis D, Piette J, Wilson BC, Golab J, Photodynamic therapy of cancer: An update. CA Cancer J. Clin 61, 250–281 (2011). [PubMed: 21617154]
75. Burnstock G, Purinergic signaling in the cardiovascular system. Circ. Res 120, 207–228 (2017). [PubMed: 28057794]
76. Hasko G, Cronstein B, Regulation of inflammation by adenosine. Front. Immunol4, 85 (2013). [PubMed: 23580000]
77. Chen ZK, Liu LL, Liang RJ, Luo ZY, He HM, Wu ZH, Tian H, Zheng MB, Ma YF, Cai LT, Bioinspired hybrid protein oxygen nanocarrier amplified photodynamic therapy for eliciting anti-tumor immunity and abscopal effect. ACS Nano 12, 8633–8645 (2018). [PubMed: 30005164]
78. Ivanova E, Kuraguchi M, Xu M, Portell AJ, Taus L, Diala I, Lalani AS, Choi J, Chambers ES, Li S, Liu S, Chen T, Barbie TU, Oxnard GR, Haworth JJ, Wong KK, Dahlberg SE, Aref AA, Barbie DA, Bahcall M, Paweletz CP, Jänne PA, Use of ex vivo patient-derived tumor organotypic spheroids to identify combination therapies for HER2 mutant non-small cell lung cancer. Clin. Cancer Res 26, 2393–2403 (2020). [PubMed: 32034078]

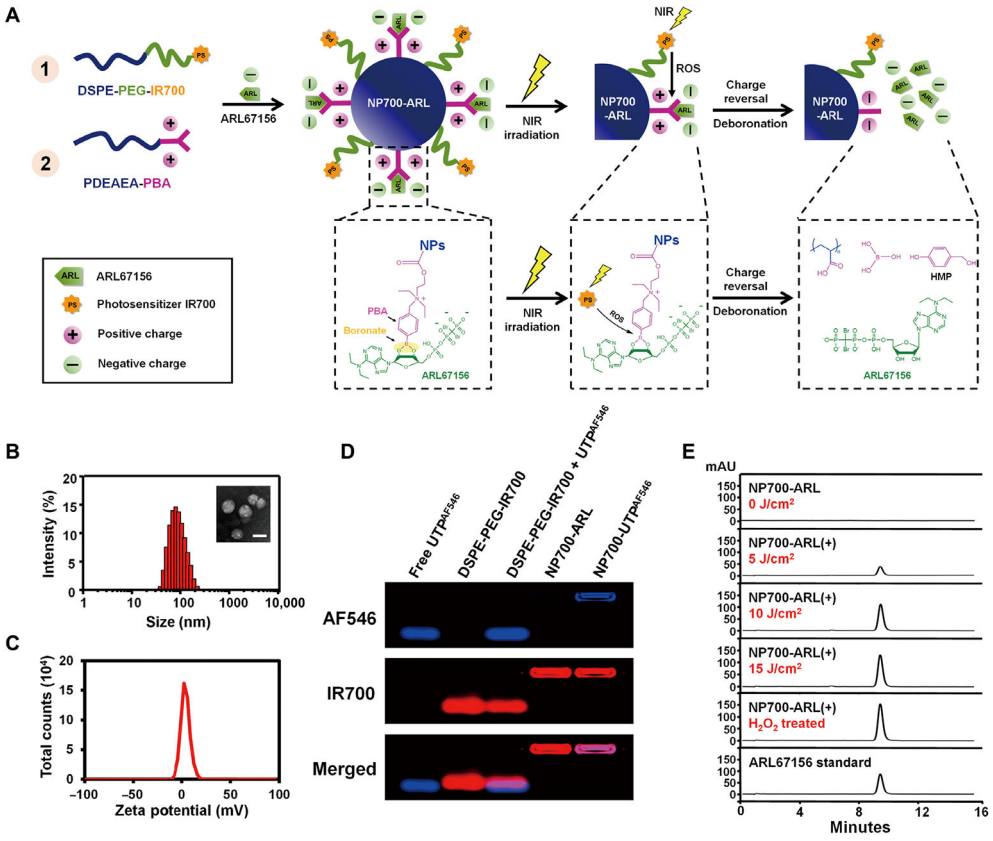

Fig. 1. Design and characterization of NP700-ARL.

(**A**) Scheme illustration of the self-assembly of NP700-ARL. In this delivery system, (1) the photosensitizer-containing lipid polymer DSPE-PEG-IR700 is a "ROS-producing" component, which damages tumor cells and induces ATP release under light irradiation; at the same time, it produces ROS as stimuli to the delivery system. (2) The BA-containing cationic polymer PDEAEA-PBA is a "ROS-responsive conjunction" component, which links the anionic nucleotides by electronic interaction and phenylboronic ester. When the lipid polymer component generating ROS undergoes NIR irradiation, the phenylboronic ester is hydrolyzed and the cationic polymer is converted into an anionic polymer, facilitating ARL67156 release in tumor sites. (**B** to **E**) Characterization of NP700-ARL. (B) Size distribution of NP700-ARL measured by dynamic light scattering (DLS). Inset: TEM image of NP700-ARL. (C) Zeta potential of NP700-ARL measured by DLS. (D) Gel retardation assay of free UTP^{AF546}, DSPE-PEG-IR700, DSPE-PEG-IR700 plus free UTP^{AF546}, NP700-ARL, and NP700-UTP^{AF546}. Red: IR700; blue: UTP^{AF546}. (E) ROS-triggered release of ARL analyzed by HPLC. The NP700-ARL was treated with 0.25 mM H_2O_2 at 37°C or irradiated with the LED light at the light doses of 5, 10, and 15 J/cm^2. The plus sign (+) indicates light irradiation.

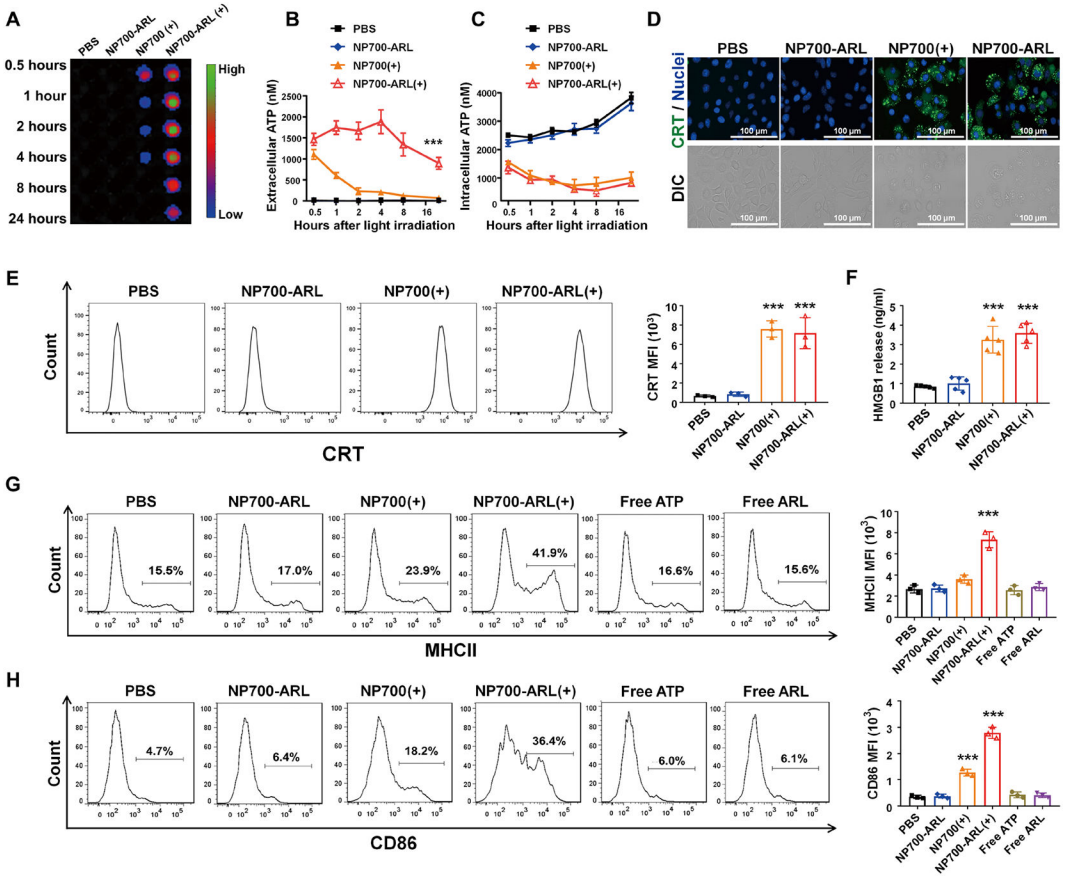

Fig. 2. NP700-ARL(+) induces ATP release and leads to immunogenic cell death of cancer cells.

(**A** to **C**) ATP release from MOC1 cells after NP700-ARL treatment followed by light irradiation. MOC1 cells were treated with different NPs with or without light irradiation at the light dose of 10 J/cm^2. Supernatants were harvested at 30 min, 1 hour, 2 hours, 4 hours, 8 hours, and 24 hours after light irradiation to detect ATP concentrations. (A) Bioluminescence image was taken after adding luciferase and luciferin to indicate eATP amounts. (B) ATP release into the supernatant or (C) residual intracellular ATP was quantified with an ATP determination kit. Two-way ANOVA repeated-measures and Tukey's multiple comparisons test were performed, ***$P < 0.001$. (**D** and **E**) Cell surface exposure of CRT after NP700-ARL(+) treatment. MOC1 cells were treated with NP700-ARL and then irradiated with the NIR light. (D) Immunostaining of CRT was performed, and the cells were imaged with fluorescence microscope. Green: CRT staining; blue: Hoechst 33342 for nuclei staining. Scale bars, 100 μm. (E) Surface translocation of CRT on the alive cells was also quantified with flow cytometry. Quantification is shown on the right. Data are shown as means ± SD of $n = 3$ biologically independent experiments. One-way ANOVA and Tukey's multiple comparisons test, ***$P < 0.001$. (**F**) Extracellular release of HMGB1 after NP700-ARL(+) treatment measured with an ELISA kit. Data are shown as means ± SD of $n = 5$ biologically independent experiments. One-way ANOVA and Tukey's multiple comparisons test, ***$P < 0.001$. (**G** and **H**) The effect of NP700-ARL(+) on DC maturation. MOC1 cells were treated with different NPs. Immature DCs were added and coincubated with the treated MOC1 cells for 24 hours. (G) The DCs were stained with anti-mouse MHC-II or

(B) anti-mouse CD86 antibodies and then analyzed by flow cytometry. Quantitative data are shown on the right. Data are shown as means ± SD of $n = 3$ biologically independent experiments. One-way ANOVA and Tukey's multiple comparisons test, ***$P < 0.001$.

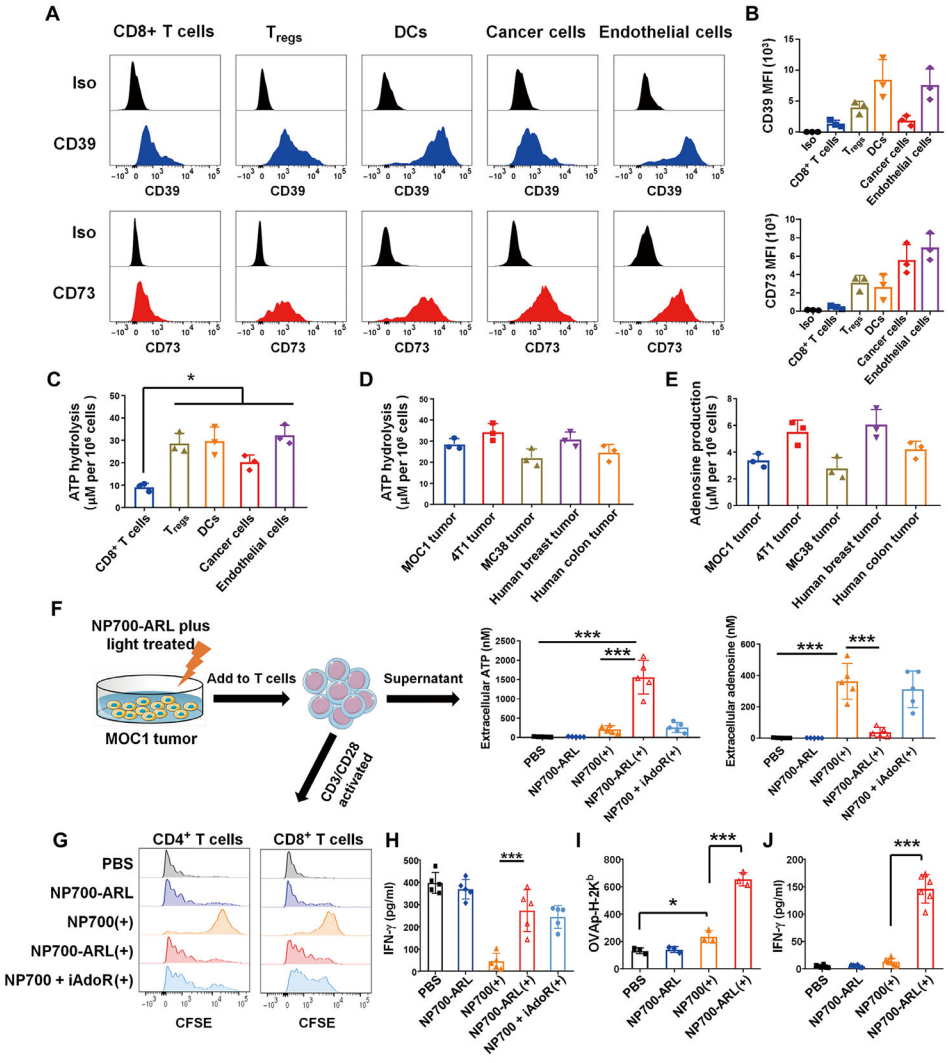

Fig. 3. NP700-ARL(+) promotes T cell proliferation and antigen-specific activation by DCs.

(**A** to **E**) Expression of CD39 and CD73 and eATP hydrolysis in the TME. (A) Flow cytometry analysis of CD39 and CD73 expression on different cell subsets from MOC1 tumors, and (B) quantification is shown on the right (data are shown as means ± SD of $n = 3$ biologically independent experiments). (C) ATP hydrolysis in different cell subsets isolated from MOC1 tumors. Cells were incubated with ATP (50 μM) at 37°C for 2 hours. Remaining eATP in the supernatant was quantified to determine the ATP hydrolyzed by ectonucleotidases. Data are shown as means ± SD of $n = 3$ biologically independent experiments. One-way ANOVA and Tukey's multiple comparisons test, $*P < 0.05$. (D and E) Enzymatic activities of CD39 and CD73 in different tumor tissues. Mouse MOC1 tumor, 4T1 tumor, MC38 tumor, and human breast or colon tumor surgical specimens were digest by collagenase IV, and then the tumor cells were incubated with ATP (50 μM) at 37°C for 2 hours. ATP and Ado in the supernatants were quantified with ATP or Ado determination kit. (D) ATP hydrolysis in different tumor tissue, and (E) Ado production in different tumor tissue. Data are shown as means ± SD of $n = 3$ biologically independent experiments. (**F**) ATP and Ado concentration in T cell culture media after

different treatments. MOC1 cells were treated with different NPs with or without light irradiation. The mixed $CD4^+$ and $CD8^+$ T cells were added to the culture and coincubated with MOC1 cells, and the remaining ATP and the Ado production were quantified. Data are shown as means ± SD of $n = 5$ biologically independent experiments. One-way ANOVA and Tukey's multiple comparisons test, $^{***}P < 0.001$. (**G** and **H**) Effect of ROS-responsive ARL delivery on T cell proliferation. The mixed $CD4^+$ and $CD8^+$ T cells were prestained with carboxyfluorescein succinimidyl ester (2 mM). After incubation with the treated MOC1 cells, the proliferation of T cells was stimulated with the addition of anti-CD3/anti-CD28–coated beads. (G) T cell proliferation was assessed with flow cytometry by quantifying the dye dilution on proliferating T cells. (H) After 48 hours, the supernatants were collected and analyzed for IFN-γ by ELISA. Data are shown as means ± SD of $n = 5$ biologically independent experiments. One-way ANOVA and Tukey's multiple comparisons test, $^{***}P < 0.001$. (**I** and **J**) Effect of NP700-ARL(+) on APC cross-presentation of tumor antigen to effector $CD8^+$ T cells. (I) MOC1-OVA cells were treated with different NPs with or without irradiation; immature DCs were added and coincubated with the treated MOC1-OVA cells. $OVA_{257–264}$ presented with MHC-I on DCs surface were detected by anti-H-$2K^b$ bound to SIINFEKL. Data are shown as means ± SD of $n = 3$ biologically independent experiments. One-way ANOVA and Tukey's multiple comparisons test, $^{*}P < 0.05$ and $^{***}P < 0.001$. (J) $CD8^+$ T cells were purified from spleens of OT-I mice and were cocultured with DCs and MOC1-OVA cells that were treated with NP700-ARL(+). After 48 hours, the supernatants were collected and analyzed for IFN-γ by ELISA. Data are shown as means ± SD of $n = 3$ biologically independent experiments. One-way ANOVA and Tukey's multiple comparisons test, $^{***}P < 0.001$.

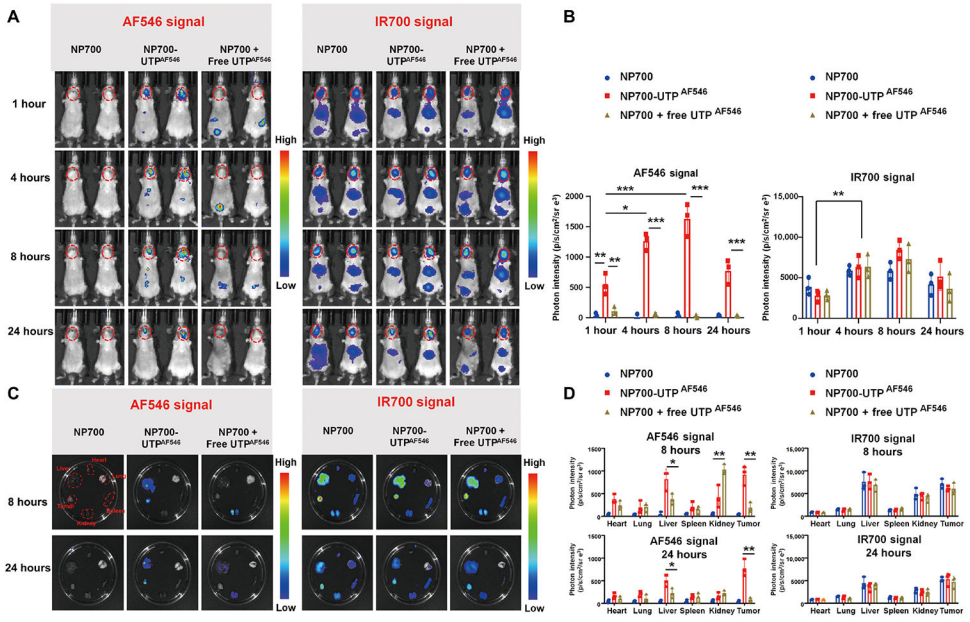

Fig. 4. NP700-based drug delivery to the tumor site in vivo.

(**A** and **B**) Biodistribution of NP700-UTP^{AF546} in MOC1 tumor–bearing mice. Mice were intravenously administered with NP700, NP700-UTP^{AF546}, or NP700 plus free UTP^{AF546}. (A) Fluorescence images were taken using an IVIS imaging system for visualization of UTP^{AF546} (left) and IR700 (right) at 1, 4, 8, and 24 hours after injection. Dotted red circles indicate tumor areas. Representative images are shown. (B) Quantification of UTP^{AF546} (left) and IR700 (right) signal intensity is shown. Data are shown as means ± SD of n = 3 biologically independent mice. One-way ANOVA and Tukey's multiple comparisons test and two-way ANOVA repeated-measures and Tukey's multiple comparisons test were performed, *P < 0.01, **P < 0.01, and ***P < 0.001. (**C** and **D**) Ex vivo biodistribution of NP700-UTP^{AF546} in main organs of MOC1 tumor–bearing mice. After imaging at 8 and 24 hours, the mice were euthanized and heart, liver, spleen, lung, kidney, and tumors were collected, and (C) were imagined with IVIS system to examine the biodistribution of the NPs in different organs based on the UTP^{AF546} signal (left) and IR700 signal (right); representative images are shown. (D) Quantification of UTP^{AF546} (left) and IR700 (right) signal intensity in different organs is shown. Data are shown as means ± SD of n = 3 biologically independent mice. One-way ANOVA and Tukey's multiple comparisons test, *P < 0.05 and **P < 0.01.

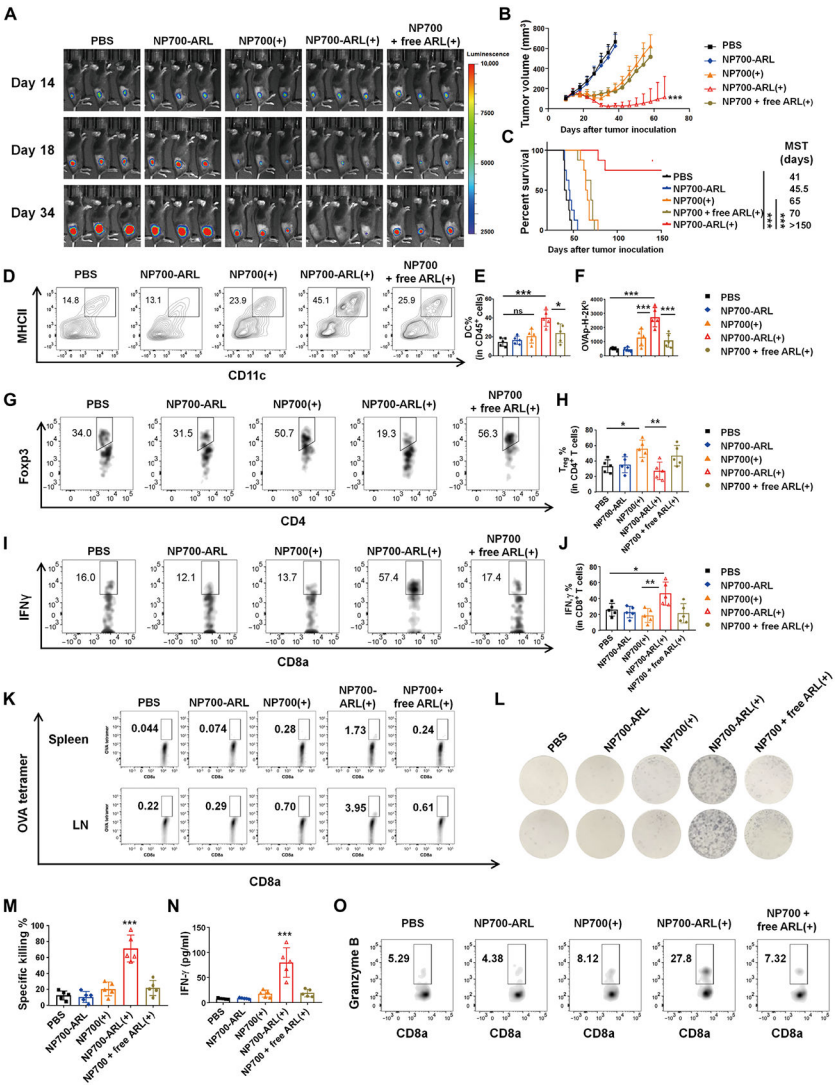

Fig. 5. NP700-ARL(+) suppresses MC38 tumor growth and induces systemic tumor-specific immunity.

(**A** to **C**) MC38-OVA-Luc tumor–bearing mice received NPs or the control agents by intravenous administration on days 14 and 17 after tumor inoculation, with or without light irradiation at tumor sites 4 hours after injection. (A) MC38-OVA-Luc tumor growth was monitored by in vivo using bioluminescence imaging. Representative images are shown. (B) MC38-OVA tumor volume was measured after different treatments. Data are shown as means ± SD of $n = 8$ biologically independent mice. Two-way ANOVA repeated-measures and Tukey's multiple comparisons test, $^{***}P < 0.001$. (C) Kaplan-Meier survival curves of indicated treatment in MC38-OVA tumor model. Data are shown as means ± SD of $n = 8$ biologically independent mice. Two-sided log-rank test, $^{***}P < 0.001$. (**D** to **J**) Effect of NP700-ARL(+) treatment on anticancer immunity in TME. The tumors were obtained from MC38-OVA mice 2 days after light irradiation and were analyzed with flow cytometry. (D) Flow cytometry analysis of $CD11c^+$ $MHC\text{-}II^+$ DCs in MC38-OVA tumors and (E) quantification of the percentages of DCs in $CD45^+$ cells in MC38-OVA tumors.(F) MFI of OVAp-H-$2K^b$ in tumors was quantified for DCs. (G) Flow cytometry

analysis of $CD4^+$ $Foxp3^+$ T_{regs} and (H) quantification of the percentages of T_{regs} in $CD4^+$ T cells in MC38-OVA tumors. (I) Flow cytometry analysis of IFN-γ^+ $CD8^+$ T cells and (J) quantification of the percentages of IFN-γ^+ T cells in $CD8^+$ T cells in MC38-OVA tumors. Data (D to J) are shown as means ± SD of $n = 5$ biologically independent mice. One-way ANOVA and Tukey's multiple comparisons test, $^*P < 0.05$, $^{**}P < 0.01$, and $^{***}P < 0.001$. (**K** and **L**) Effect of NP700-ARL(+) treatment on systemic tumor-specific immunity. (K) Flow cytometry analysis of spleen (top) and TDLNs (bottom) for SIINFEKL tetramer$^+$ OVA-specific $CD8^+$ T cells from the MC38-OVA tumor–bearing mice treated with indicated groups. (L) ELISpot analysis of IFN-γ spot forming cells from splenocytes after ex vivo restimulation with SIINFEKL peptide. Splenocytes were collected 14 days after light irradiation. Two representative spots per group were shown. (**M** to **O**) Ex vivo cytotoxicity of tumor-infiltrating $CD8^+$ T cells. $CD8^+$ T cells isolated from MC38-OVA-Luc tumors of the C57BL/6 mice receiving different treatments and then cocultured with MC38-OVA-Luc tumor cells at target-to-effector ratio of 20:1. (M) Tumor-specific cell killing was quantified by luciferase assay. (N) IFN-γ production of tumor-infiltrating $CD8^+$ T cells was measured by ELISA assay. Data are shown as means ± SD of $n = 5$ biologically independent mice. One-way ANOVA and Tukey's multiple comparisons test, $^{***}P < 0.001$. (O) Flow cytometry analysis of $CD8^+$ T cells for cytotoxic protease Granzyme B.

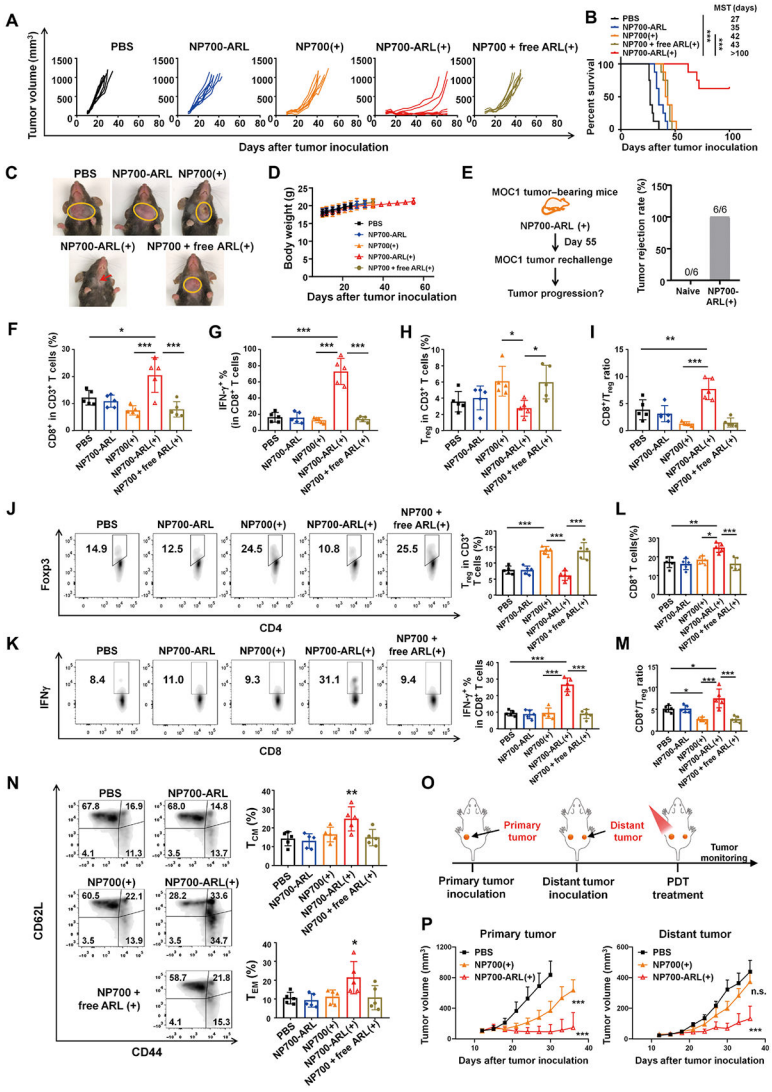

Fig. 6. NP700-ARL(+) inhibits MOC1 tumor growth and stimulates anticancer immunity.

(**A** to **E**) MOC1 tumor–bearing mice received indicated treatments on days 12 and 15 after tumor inoculation. (A) MOC1 tumor growth curves in individual animals were measured, n = 8 biologically independent mice. (B) Kaplan-Meier survival curves of indicated treatments in MOC1 tumor model. Data are shown as means ± SD of n = 8 biologically independent mice. Two-sided log-rank test, $***P < 0.001$. (C) The mice were imaged on day 24, with the tumor sites indicated with yellow circles. Representative images are shown. (D) Body weights of mice receiving different treatments from days 6 to 55. Data are shown as means ± SD of n = 8 biologically independent mice. (E) Mice cured with NP-ARL(+) were rechallenged 55 days later with MOC1 tumor cells. Naïve mice were challenged at the same time served as control. Data showed the percent of mice rejecting MOC1 tumor rechallenge, n = 6 biologically independent mice. (**F** to **I**) Effect of NP700-ARL(+) treatment on anticancer immunity in MOC1 tumors. The tumors were obtained 2 days after light irradiation and were analyzed with flow cytometry. Quantitative analysis of percentage of (F) $CD8^+$ T cells, (G) IFN-γ^+ $CD8^+$ T cells, (H) $CD4^+Foxp3^+$ T_{regs}, and

(I) the ratio of $CD8^+$ T cells/T_{regs} in tumors. Data are shown as means ± SD of $n = 5$ biologically independent mice. One-way ANOVA and Dunnett's multiple comparisons test compared with NP700-ARL(+) group, $^{**}P < 0.01$ and $^{***}P < 0.001$. (**J** to **M**) Effect of NP700-ARL(+) treatment on anticancer immunity in TDLNs. The TDLNs were obtained 2 days after light irradiation from the mice and were analyzed with flow cytometry. (J) Representative flow cytometry analysis of $CD4^+Foxp3^+$ T_{regs} in TDLNs, and quantification data are shown on the right. (K) Representative flow cytometry analysis of IFN-γ^+ $CD8^+$ T cells in TDLNs, and quantification data are shown on the right. (L) Quantitative analysis of the percentage of $CD8^+$ T cells in TDLNs. (M) Quantitative analysis of the ratio of $CD8^+$ T cells/T_{regs} in TDLNs. Data for quantitative analysis are shown as means ± SD of $n = 5$ biologically independent mice. One-way ANOVA and Tukey's multiple comparisons test, $^{*}P < 0.05$, $^{**}P < 0.01$, and $^{***}P < 0.001$. (**N**) Representative flow cytometry analysis of memory T (Tm) cells in TDLNs from different treatment groups, and quantification data are shown on the right. The percentage of central Tm (T_{CM}) cells and effector Tm (T_{EM}) cells were calculated based on CD44 and CD62L surface expression. Data for quantitative analysis are shown as means ± SD of $n = 5$ biologically independent mice. One-way ANOVA and Dunnett's multiple comparisons test compared with the PBS group, $^{*}P < 0.05$ and $^{**}P < 0.01$. (**O** and **P**) Abscopal effect of NP700-ARL(+) in MOC1 tumor model. (O) A schematic to illustrate the experimental procedures to evaluate the abscopal effect induced by NP700-ARL–mediated PDT. Primary MOC1 tumor cells were inoculated at left flank of C57bl/6 mice at day 0, and the distant tumor was inoculated at right flank of the same mouse at day 8; mice received different treatments on days 12 and 15. (P) Growth curves of primary tumor and distant tumor were monitored after indicated treatments. Data are shown as means ± SD of $n = 8$ biologically independent mice. Two-way ANOVA repeated-measures and Tukey's multiple comparisons were test performed, $^{***}P < 0.001$.

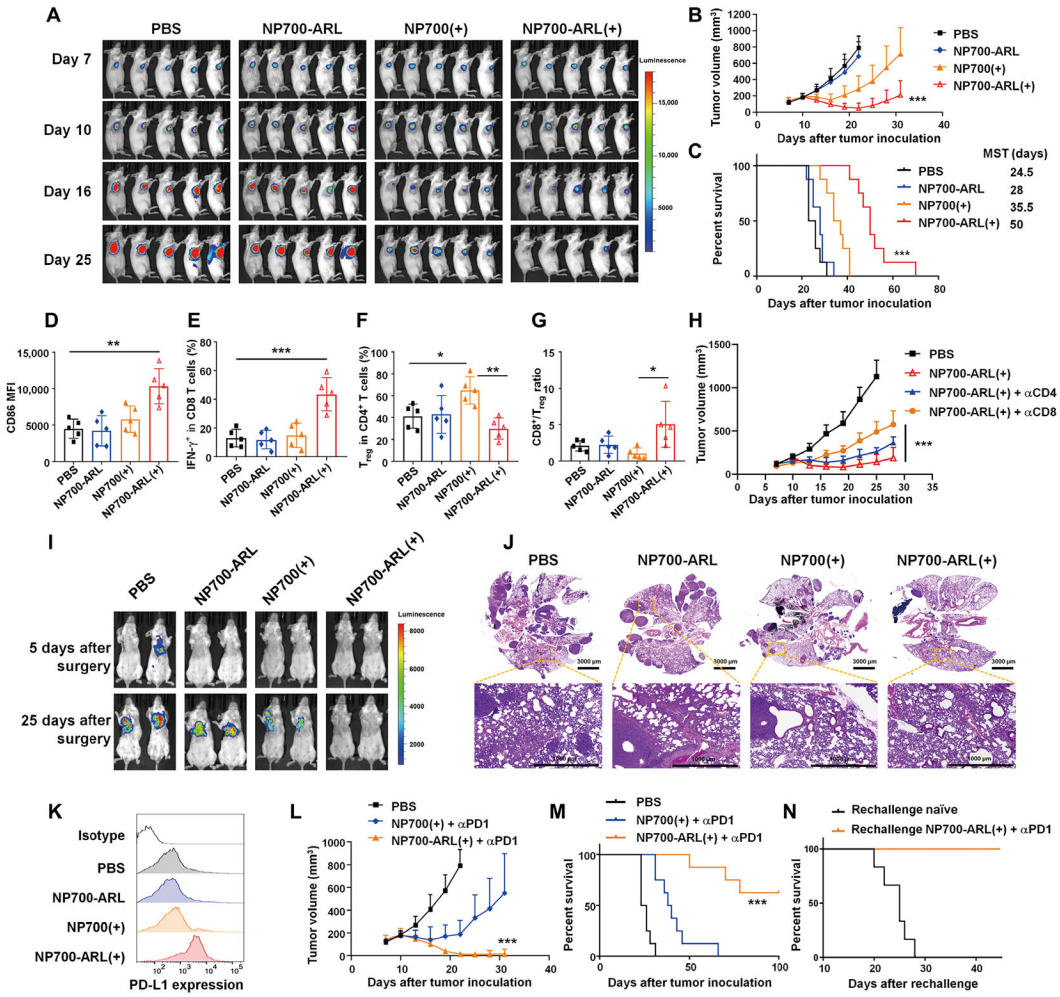

Fig. 7. NP700-ARL(+) suppresses 4T1 tumor growth and reduces its metastasis to lung.

(**A** to **C**) 4T1-Luc tumor–bearing mice received indicated treatments on days 10 and 13. (A) Tumor growth was monitored by in vivo bioluminescence imaging for different treatment groups (five representative mice shown per group). (B) Tumor volume was measured following indicated treatments. Data are shown as means ± SD of $n = 8$ biologically independent mice. Two-way ANOVA repeated-measures and Tukey's multiple comparisons test, $***P < 0.001$. (C) Kaplan-Meier survival curves of indicated treatments in 4T1-Luc tumor model. Data are shown as means ± SD of $n = 8$ biologically independent mice. Two-sided log-rank test, $***P < 0.001$. (**D** to **G**) NP700-ARL(+) stimulated anticancer immunity in 4T1-Luc tumors. Tumors were collected 2 days after light irradiation and were analyzed with flow cytometry. (D) Quantitative analysis of the CD86 MFI of $CD11c^+$ and $MHC\text{-}II^+$ DCs in tumors. (E) Quantitative analysis of the percentage of IFN-γ^+ $CD8^+$ T cells in tumors. (F) Quantitative analysis of the percentage of $CD4^+Foxp3^+$ T_{regs} in tumors. (G) Quantitative analysis of the ratio of $CD8^+$ T cells/T_{regs} in tumors. Data are shown as means ± SD of $n = 5$ biologically independent mice. One-way ANOVA and Tukey's multiple comparisons test, $*P < 0.05$, $**P < 0.01$, and $***P < 0.001$. (**H**) $CD8^+$ and $CD4^+$ T cell depletion study. The 4T1 tumor–bearing mice receiving the NP700-ARL(+) were depleted of $CD4^+$ or $CD8^+$ T cells by injection of depletion antibodies twice per week. Tumor volume

was measured and shown. Data are shown as means ± SD of $n = 8$ biologically independent mice. Two-way ANOVA repeated-measures and Tukey's multiple comparisons test, ***$P < 0.001$. (**I**) The lung metastasis of 4T1-Luc was monitored by in vivo bioluminescence imaging at days 5 or 25 after the primary tumor was surgically removed. Two representative mice of $n = 4$ mice per group are shown per group. (**J**) Representative H&E sections of lung tissue from indicated treatment. Scale bars, 3000 μm (top) and 1000 μm (bottom). (**K** to **N**) The combination therapy of NP700-ARL(+) with anti-PD1 antibody therapy in 4T1-Luc model. (K) The PD-L1 expression of 4T1-Luc tumor cells was analyzed by flow cytometry 4 days after light irradiation. (L) Tumor volume was measured after NP700-ARL(+) plus anti-PD1 antibody treatment. Data are shown as means ± SD of $n = 8$ biologically independent mice. Two-way ANOVA repeated-measures and Tukey's multiple comparisons test, ***$P < 0.001$. (M) Kaplan-Meier survival curve of NP700-ARL(+) plus anti-PD1 antibody in 4T1-Luc tumor model. Data are shown as means ± SD of $n = 8$ biologically independent mice. Data were analyzed by two-sided log-rank test, ***$P < 0.001$. (N) Kaplan-Meier survival curve after 4T1-Luc tumor rechallenge. Mice cured with the combination therapy ($n = 5$) were rechallenged on day 100. Naïve mice ($n = 6$) that were challenged at the same time served as control.